Asian Journal of Chemistry; Vol. 29, No. 2 (2017), 242-256

ASIAN JOURNAL OF CHEMISTRY

http://dx.doi.org/10.14233/ajchem.2017.20148

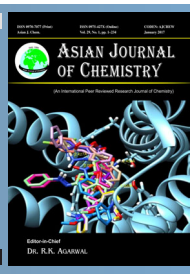

Vibrational Spectroscopic and Molecular Docking Studies on N-Carbobenzoxy-L-2-phenylglycine by Density Functional Theory Method

M. SATHISH[1,2,*], G. MEENAKSHI[3], S. XAVIER[2], S. SEBASTIAN[2] and V. SATHANA[2]

[1]Manonmaniam Sundaranar University, Tirunelveli-627 012, India
[2]Department of Physics, St. Joseph's College of Arts & Science (Autonomous), Cuddalore-607 001, India
[3]Department of Physics, Kanchi Mamunivar Center for Post Graduate Studies and Research, Puducherry-605 008, India

*Corresponding author: E-mail: marysathish2013@gmail.com

Received: 20 June 2016; *Accepted*: 19 September 2016; *Published online*: 30 November 2016; AJC-18138

The NLO compound, N-carbobenzoxy-L-2-phenyl glycine (CbzLPG) has been characterized by Fourier transform infrared, Fourier transform Raman and ultraviolet-visible spectrometry. Density functional theory (DFT) calculations has been carried out by performing DFT-B3LYP and M06-2X levels of theories using 6-311+G(d,p) basis set. The geometry of the structure was optimized without any symmetry constraints using the DFT-B3LYP/M06-2X with 6–311+G(d,p) levels of estimations. The targeted interpretation of the vibrational spectra has been prepared on the basis of the calculated potential energy distribution matrix (PED). The vibrational frequencies decided tentatively are contrasted and those acquired hypothetically from DFT computations employing the B3LYP/6–311+G(d,p) and M06-2X/6–311+G(d,p) methods for the optimized geometry of the compound. Utilizing the natural bond orbital (NBO) evaluation stability of the analysis steadiness of the molecule emerging from hyper conjugative interactions, charge delocalization has been examined. In addition, frontier molecular orbitals and molecular electrostatic potential were computed by way of utilizing density functional theory (DFT/B3LYP) using 6-311+G(d,p) basis set. The computed HOMO and LUMO energies demonstrate that charge exchange happens inside of the molecule. The structure-substance reactivity relations of the compound were resolved through global and local reactivity descriptors by conceptual DFT methods. The first order hyperpolarizability (β_0) and related properties (β, α_0 and $\Delta\alpha$) of N-carbobenzoxy-L-2-phenyl glycine were calculated. Thermodynamic functions of a label compound were furthermore carried out from B3LYP with basis set 6-311+G(d,p) using Thermo.pl software. As a result, the performances of the B3LYP method with the prediction of the wavenumbers within the molecule were quite close. Molecular docking studies of N-carbobenzoxy-L-2-phenyl glycine has been performed and analyzed.

Keywords: N-Carbobenzoxy-L-2-phenylglycine, TD-DFT, Natural bond orbital.

INTRODUCTION

Phenylglycine, the easiest fragrant amino acid is fascinating since of its advantage purposes as medical agents involved in the alkali ions transport within the biological and clinical methods. L-Phenylglycine has a pharmacologic and analgesic efficacy profile similar to that of pregabalin and gabapentin [1]. Phenylglycine (PGLY) is a non-protein amino acid, which currently attracts concentration for its function in antitumor and neuropathic drug synthesis and for its lately said genotoxic endeavor [1,2]. The benzyloxycarbonyl group (Cbz) has been widely used to protect amino groups in organic synthetic reactions. Phenylalanine, the easiest protein fragrant amino acid, is highly hydrophobic. Phenylglycine, fundamentally the same in structure to phenylalanine gave off an impression of being an essential beginning material underway of the β-lactam drugs, *e.g.*, semisynthetic penicillins and cephalosporins where it makes side chain as for instance in ampicillin, cephalexin or cephalor. L-Phenylglycine has a pharmacologic and analgesic efficacy profile similar to that of pregabalin and gabapentin. Phenylglycine and L-phenylglycine drugs are widely used to relieve mostly neuropathic pain. Our molecule N-carbobenzoxy-L-2-phenylglycine is one of the N-protected amino acids derivatives. It has the accompanying properties; Appearance: white solid; m.f.: $C_{16}H_{15}NO_4$; m.w.: 285.30 g/mol; m.p.: 131 °C.

Despite the fascinating properties of phenylglycine, rather rare structural and spectroscopic information concerning this molecule or its subordinates are accessible in the writing. Crystal structures of six phenylglycine salts with various inorganic acids have been studied [3-8]. Recently identification and functional characterization of phenylglycine have been reported by Mast *et al.* [9]. Kusano *et al.* [10] analyzed synthesis of N-carbobenzoxy-L-aspartyl-L-phenylalanine methyl ester catalyzed by thermolysin variants with improved activity. Ilczyszyn *et al.* [11,12] reported structural, vibrational and

theoretical studies of sodium DL-phenylglycinate trihydrate and potassium DL-phenylglycinate.

In view of the cited works, it's unmistakable that there's no quantum mechanical learn on this title molecule which has impelled to do a definite quantum mechanical examination for understanding the comprehension the vibrational modes, chemical shifts, HOMO-LUMO, MEP and thermodynamic properties of title compound. In this work, the structural and vibrational investigations of a basic N-carbobenzoxy-L-2-phenylglycine was introduced and discussed. The point of these computations was triple: an examination between the exploratory structural parameters decided from the X-ray investigation and hypothetical geometry parameters, supporting the infrared and Raman spectra by the examination with the hypothetical vibrational information and the endeavor to reproduce the exploratory spectra of the N-carbobenzoxy-L-2-phenyl glycine (CbzLPG). The calculations were performed at the M06-2X and B3LYP/6-311+G(d,p) level with the intention of comparing the structural parameters and helping the vibration modes undertaking. The electronic dipole moment (μ) and first order hyperpolarizability (β) value of the molecule have been computed using *ab initio* DFT method to study the NLO property. Natural bond orbital (NBO) analysis was performed to provide valuable information about various intermolecular interactions. The figured HOMO and LUMO energies demonstrate that charge flow in the molecule in the molecule. Finally electronegativity (χ), hardness (η), softness (S), molecular electrostatic potential maps (MEP) and thermodynamic properties were calculated.

EXPERIMENTAL

The compound N-carbobenzoxy-L-2-phenylglycine in the solid form was obtained from TCI INDIA synthetic organization at Chennai, with an expressed virtue more prominent than 98 % and used as supplied. BRUKER Optik GmbH FT-IR spectrometer has been used to record the FT-IR spectrum using KBr pellet technique at room temperature. The spectral range is 4000-400 cm^{-1}. BRUKER RFS 27: FT-Raman spectrometer equipped with FT-Raman module accessory was used to record FT-Raman spectrum of the CbzLPG compound using 1064 nm line of Nd:YAG laser as excitation wavelength within the spectral range 3500-50 cm^{-1}. The laser output was held in 100 mW because of its solid sample. Cary 500 UV-VIS-NIR spectrometer was used to record the UV absorption spectra associated with CbzLPG were examined with the range 200-800 nm. The UV pattern is usually acknowledged from the 10-5 molar solution connected with CbzLPG, dissolved with ethanol solvent.

COMPUTATIONAL METHODS

In recent years, an interest in the usage of DFT approaches in one of a kind varieties of applications, principally for the reason that the introduction of accurate non-local corrections. In DFT thought, exchange-correlation energy is the major predicament among the entire approximations consequently; the accuracy of DFT is depended straight *via* the approximate nature of the exchange-correlation energy functional. The DFT approaches employed in the present paper are consultant in aspect of the exchange-correlation energy and were frequently utilized in various hypothetical studies [13-21]. The excessive parameterized, empirical exchange correlation functionals, M05-2X and M06-2X, developed by Zhao and Truhlar [22] have been shown to explain non-covalent interactions better than density functional which might be presently in fashioned use. Nevertheless, these ways have yet to be totally benchmarked for the forms of interactions main in biomolecules. M05-2X and M06-2X are claimed to seize ''medium-range'' electron correlation. However, the long-range'' electron correlation uncared for by way of these functional may also be fundamental in the binding of non-covalent elaborate. Additionally, these approaches have been utilized in countless theoretical reports [23-29]. The vibrational frequencies and geometrical parameters were calculated at B3LYP and M06-2X/6–311+G(d,p) level of calculations with the Gaussian 09 program [30]. The molecular structure optimization and corresponding vibrational harmonic frequencies had been calculated utilizing DFT calculations [31] with the Becke's three-parameter hybrid functional (B3) [32] for the alternate section and the Lee-Yang-Parr (LYP) correlation function [33], for the computation of molecular structure, vibrational frequencies and energies of optimized structures *via* utilizing Gaussian 09 suite of quantum chemical codes. First of all, the title molecule was once optimized, after then the optimized parameters were used in the vibrational frequency and calculations of electronic properties. The vibrational wavenumber assignments were applied by using combining the outcome of the Gauss view 5.08 [34] and VEDA4 applications [35]. Calculation of theoretical vibrational spectra utilizing a type of quantum mechanical application enabling use of a sort of quantum chemical procedures based on perturbation, density functional methods. The most of vibrational spectra are still calculated within the harmonic approximation generating some systematical mistakes. Commonly, there are two methods to interpret a theoretical vibrational spectrum of a molecule: a visualization of the atom motion and potential energy distribution (PED) analysis [36-41]. VEDA software for PED analysis of theoretical vibrational spectra is described. VEDA internal coordinates centered on molecular structure. Potential energy distribution evaluation is indispensible in modern-day vibrational spectroscopy laboratories [42]. The calculated IR spectrum plotted utilizing the pure Lorentzian band form with a band width of FWHM of 10 cm^{-1} has been used when put next with the experimental IR spectrum. The normal bonding orbital (NBO) calculations [43] had been carried out making use of Gaussian 09 [30] package on the same stage in order second order interactions between the stuffed orbitals of one subsystem and vacant orbitals of a different subsystem, which is a measure of the intermolecular delocalization or hyper conjugation. UV-visible spectra (ethanol solvent), electronic transitions, vertical excitation energies absorbance and oscillator strengths have been computed with the time-dependent DFT process. The electronic properties such as HOMO and LUMO energies had been decided by using TD-DFT approach. To examine the reactive sites of the title compound the MEP was evaluated utilizing the B3LYP process. The changes in the thermodynamic features (the heat capacity, entropy, entropy and enthalpy) had been investigated

for the different temperatures from the vibrational frequency calculations of molecule. The first order hyperpolarizability (β_0) of this molecular system and related properties (β, α_0 and $\Delta\alpha$) of are calculated using 6–311+G(d,p) basis set, based on the finite-field approach [44].

Prediction of Raman intensities: The Raman activities (S_i) determined simply by Gaussian 09 [30] has been converted to relative Raman intensities (I^R). The theoretical Raman intensity (I^R), which simulates the measured Raman spectrum, is given by the equation [45,46]:

$$I_i^R = C (\nu_0 - \nu_i)^4 \nu_i^{-1} B_i^{-1} S_i \quad (1)$$

$$B_i = 1 - (\exp h\nu_i c/kT) \quad (2)$$

The theoretical Raman spectra have been calculated by the Raint program [47].

RESULTS AND DISCUSSION

Conformational stability: Keeping in mind the end goal to depict conformational adaptability of the title atom, the vitality profile as a function of C15-O14-C12-N2 torsion angle was achieved with B3LYP/6-311+G(d,p) level of calculation to arrive the reliable conformation about dihedral angle between the two ring systems C15-O14-C12-N2. Fig. 1 shows a one-dimensional relaxed scan of the C15-O14-C12-N2 dihedral angle using the B3LYP/6-311+G(d, p) level of calculation. During the calculation, all the geometrical parameters were simultaneously relaxed, while the C15-O14-C12-N2 angle was varied in steps of 10°, 20°, 30° ... 360°. While performing the scan, the program searched for a minimum point for each 10°. For the C15-O14-C12-N2 torsion angle the minimum energy was obtained at 0.0° and 360°. Further results are based on the most stable conformer of molecule CbzLPG to clarify molecular structure and assignments of vibrational spectra.

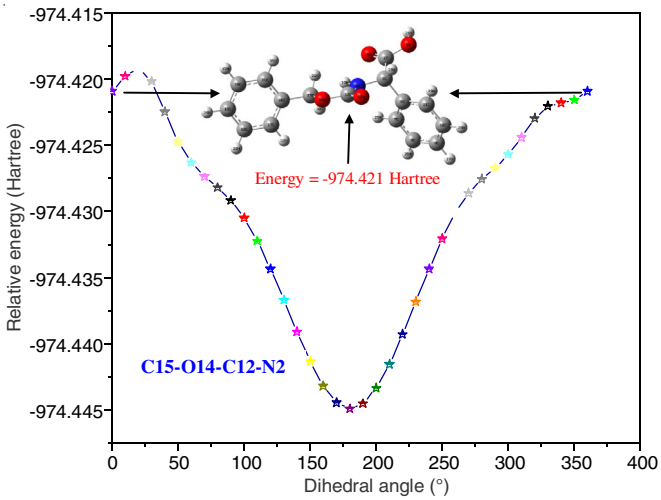

Fig. 1. Dihedral angle-relative energy curves of the N-carbobenzoxy-L-2-phenylglycine by B3LYP/6-311+G (d,p) level of theory

Structural analysis: The optimized molecular structure of CbzLPG was shown in Fig. 2. The optimized geometrical parameters (bonds lengths, bond angles and dihedral angles) obtained by the B3LYP and M06-2X/6-311+G(d,p) basis set calculations have been provided in supporting information 1. The molecular structure of the title molecule in the ground

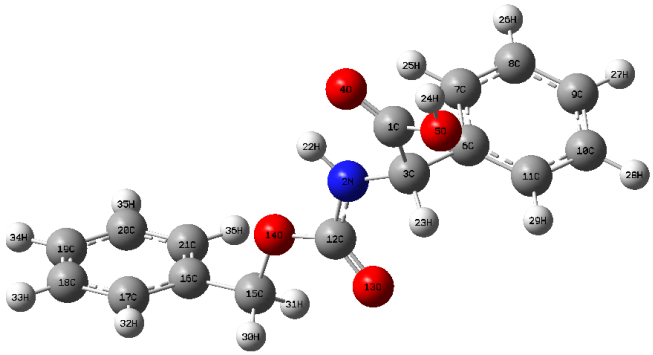

Fig. 2. Optimized molecular structure and atomic numbering of N-carbobenzoxy-L-2-phenylglycine

state (in gas phase) has been optimized with the aid of making use of DFT/B3LYP and M06-2X approaches with 6-311+G(d,p) level of calculations and the determined optimized composition has become utilized in vibrational frequency calculations. To best of our knowledge, the XRD crystal structure data of the title compound is not yet reported. Our molecule CbzLPG is compared with XRD data of closely related molecules DL-phenylglycinium chloride [8] and methyl 1-[(Z)-2-(benzyloxycarbonyl)hydrazin-1-ylidene]-5-chloro-2-hydroxy-indane-2-carboxylate [48].

The optimized bond lengths of C–C in phenyl rings falls in the range from 1.390 Å to 1.396 Å by M06-2X level of calculation and 1.393 Å to 1.398 Å by B3LYP level of calculation, which are in good agreement with XRD values [1.347-1.382 Å]. The C–C bond length of the benzene ring is not same, this is due to the *meta* substituent of the CH and CH_2 substituent on the 5th and 16th carbon atoms of the phenyl ring I and II, respectively. The bond length of C6–C7 = 1.396 Å (M06-2X)/1.397 Å (B3LYP)/1.385 Å (XRD) and C6–C11 = 1.393 Å (M06-2X)/1.395 Å (B3LYP)/1.391 Å (XRD), which is greater than the C7–C8 = 1.390 Å (M06-2X) 1.393 Å (B3LYP)/1.382 Å (XRD) at the rest of the substituent, the reason for the elongation of these bond lengths are due to the substitution of the CH group of the phenyl ring I. Due to the CH_2 meta substitution on the phenyl ring II, same trend is observed, the bond length of C16–C17 = 1.393 Å (M06-2X)/1.397 Å (B3LYP)/1.362 Å (XRD) and C16–C21 = 1.396 Å (M06–2X)/1.398 Å (B3LYP)/1.374 Å (XRD), which is greater than the C18–C19 = 1.391 Å (M06-2X)/1.394 Å (B3LYP)/1.347 Å (XRD) at the rest of the substituent. The aromatic C–H bond lengths varies from 1.085-1.088 Å/1.084-1.085 Å are calculated by M06-2X/B3LYP level of calculation, respectively, which is good agreement with observed XRD value at 0.930 Å. On the other hand small increments occur in the CH_2 and CH group bond lengths. For example CH_2 and C–H group bond lengths are C15-H30 = 1.095 Å/1.092 Å, C15-H31 = 1.095 Å/1.091 Å and C3-H23 = 1.095 Å/1.092 Å calculated by M06-2X/B3LYP level of calculations, respectively. As oxygen is more electronegative than carbon, the electrons in the C=O bond are drawn towards the oxygen. This means that carbonyl compounds are polar and have substantial dipole moments. The C12=O13 bond is short 1.214 Å (M06-2X, B3LYP)/1.206 Å (XRD). Due to pulling of electron from carbon C15, the bond strength changes which results in the lengthening of the bond C15–C16=1.504 (M06-2X)/1.503 Å (B3LYP)/1.495 Å (XRD)

compared with benzene C–C bonds. The other bond lengths are presented in Table-1. In the theoretical ideals, all of us located which a lot of the optimized bond lengths are generally slightly higher than the experimental values because of undeniable fact that the hypothetical counts have a place with detached molecule in vaporous stage and the experimental results fit in with molecules in solid state. With the electron donating substituent on the benzene ring, the symmetry of the rings are distorted, yielding to ring angles smaller than (120°) at the points of substitution. Due to the electron donating effect of CH and CH_2 group, it is observed that the bond angles at the point of substitution on phenyl rings I and II are C7–C6–C11 = 119.8° (M06-2X)/119.4° (B3LYP)/119.5° (XRD) and C17–C16–C21=119.3° (M06-2X)/118.9° (B3LYP)/117.9° (XRD). This indicates that the inner bond angle is less than 120°.

The torsion angle between the phenyl ring II and CH_2 is C15-C16-H21-C20 = -117.7°/-179.35° calculated by M06-2X and B3LYP level of calculation, respectively, which is in good agreement with experimental values –174.7°. The branched-chain torsion angle N2-C12-O14-C15 = -177.9°/-179.9°/–179.1° observed by M06-2X/B3LYP/XRD, respectively, this indicates a folded conformation of the title molecule. The folded configuration of title molecule is C12-N2-C3-C1 torsion angle, which are calculated -162.2/-150.59 by M06-2X/B3LYP, respectively. The torsion angle between the phenyl ring I and CH are H23-C3-C6-C7 = -164°/169.15° calculated by M06-2X and B3LYP level of calculation, respectively.

Vibrational spectral analysis: The experimental FT-IR spectrum of the title compound is compared the chosen theoretical spectra in Figs. 3 and 4. The scaled calculated harmonic vibrational frequencies at both B3LYP and M06-2X levels, observed vibrational frequencies and detailed PED assignments are tabulated in Table-1. The main focus on the present investigation is the proper assignment of the experimental frequencies to the various vibrational modes of CbzLPG in collaboration with the scaled down calculated harmonic vibrational frequencies at B3LYP and M06-2X levels using 6-311+G(d,p) basis set.

Comparison involving these frequencies computed on M06-2X, B3LYP level while using the hypothetical and experimental ideals discloses overestimation on the computed vibrational processes on account of neglect of anharmonicity in real system. Addition involving electron relationship inside B3LYP stage of calculation to some degree makes this regularity ideals smaller in comparison with M06-2X regularity. We all know that DFT potentials systematically overestimate this vibrational wavenumbers; these discrepancies are corrected either *via* computing anharmonic corrections explicitly or through introducing scaled factor or straight scaling the calculated the calculated wavenumber with the proper factor. The scale factors used in this study minimized the deviations very much between the computed and experimental frequencies at B3LYP method of calculation. The scale factor 0.93, 0.95, 0.9688 are used in B3LYP/6-311+G(d,p) for N–H stretching, C–H/C=O stretching and all other vibrations [49], respectively and 0.9701 M06-2X/6-311+G(d,p) method [50]. After scaling with the scaling factor, the deviation from the experimental is less than

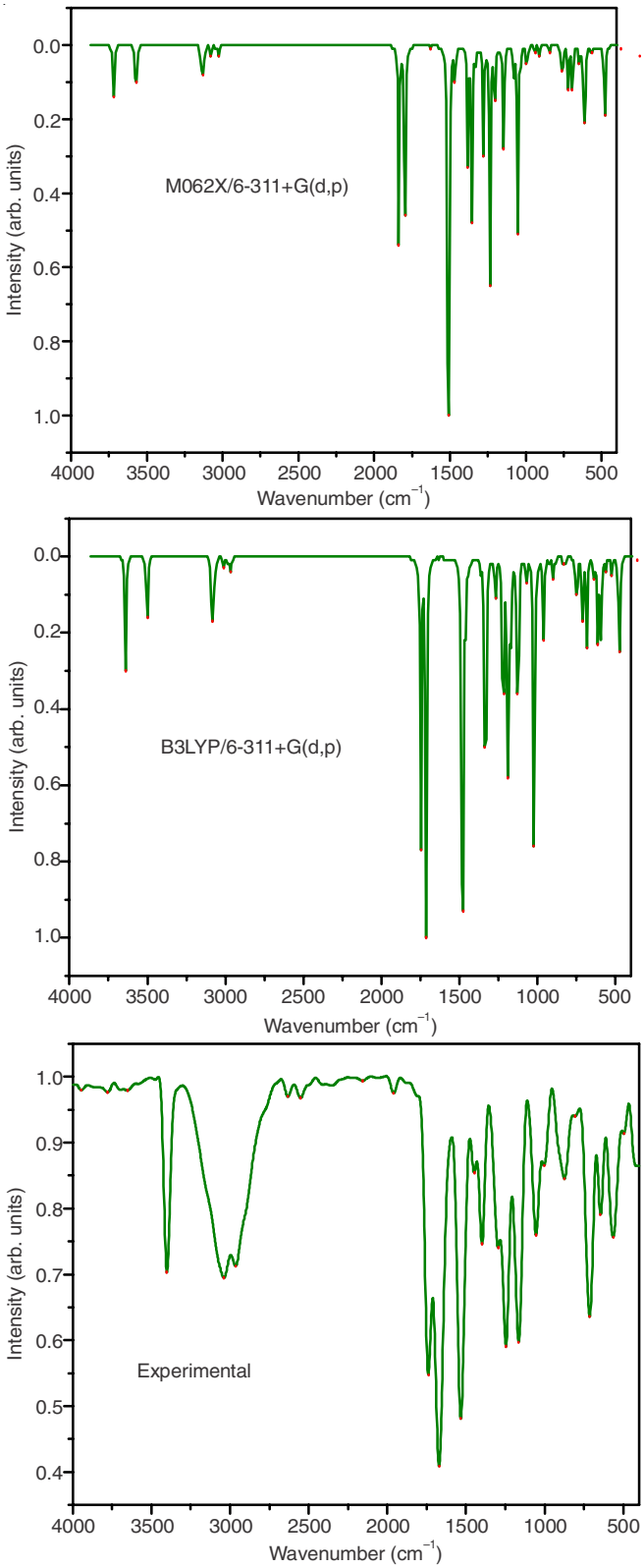

Fig. 3. Comparison of theoretical M06 2X/6-311+G (d,p) and B3LYP/6-311+G (d,p) and experimental FT-IR spectra for N-carbobenzoxy-L-2-phenylglycine

10 cm^{-1} with few exceptions. According to theoretical calculations, studied CbzLPG molecule has assumed to possess a planar structure of C_1 point group symmetry. The 102 normal modes of vibrations are distributed as 35 stretching modes, 34 bending modes and 33 torsional modes considering C_1 symmetry. All

TABLE-1
COMPARISON OF THE EXPERIMENTAL AND CALCULATED VIBRATIONAL SPECTRA AND PROPOSED ASSIGNMENTS OF N-CARBOBENZOXY-L-2-PHENYLGLYCINE

Mode No.	Experimental wavenumber (cm^{-1})		Theoretical wavenumber (cm^{-1})								PED (≥ 10 %) with assignments
	FT-IR	FT-Raman	M062X/6-311 + G(d,p)				B3LYP/6-311 + G(d,p)				
			Unscaled	Scaled	$^{a}I_{IR}$	$^{b}I_{RA}$	Unscaled	Scaled	$^{a}I_{IR}$	$^{b}I_{RA}$	
1	3652m		3833	3718	30.03	0.01	3756	3639	23.84	2.85	$\nu_{OH(100)}$
2	3402m		3680	3570	23.97	0.01	3616	3363	18.66	1.08	$\nu_{NH(100)}$
3		3063w	3242	3145	2.87	0.01	3192	3032	3.27	10.20	$\nu_{CH(85)\ Ph\ I}$
4			3234	3137	2.06	0.01	3190	3031	3.58	9.58	$\nu_{CH(100)\ Ph\ II}$
5			3232	3136	5.22	0.02	3183	3024	5.76	0.54	$\nu_{CH(88)\ Ph\ I}$
6			3228	3131	4.61	0.03	3180	3021	7.11	0.98	$\nu_{CH(100)\ Ph\ II}$
7			3224	3128	2.64	0.04	3176	3017	2.63	2.25	$\nu_{CH(80)\ Ph\ I}$
8			3219	3122	2.88	0.04	3171	3012	2.42	3.17	$\nu_{CH(85)\ Ph\ II}$
9			3214	3118	0.09	0.04	3169	3011	0.08	3.08	$\nu_{CH(77)\ Ph\ I}$
10			3212	3116	0.02	0.04	3163	3005	0.33	0.65	$\nu_{CH(82)\ Ph\ I}$
11			3208	3112	1.29	0.06	3162	3004	0.51	2.95	$\nu_{CH(85)\ Ph\ II}$
12	3039w	2992w	3205	3110	0.02	0.06	3159	3001	1.06	0.40	$\nu_{CH(86)\ Ph\ II}$
13			3171	3076	3.19	0.06	3107	2952	2.89	1.05	$\nu_{asymCH(99)\ CH2}$
14			3140	3046	1.65	0.06	3079	2925	2.03	1.57	$\nu_{C3H23(99)}$
15	2964w	2961w	3115	3022	4.49	0.08	3060	2907	4.60	3.23	$\nu_{symCH(98)\ CH2}$
16	1739m	1734w	1893	1837	62.98	0.09	1805	1715	63.33	1.69	$\nu_{O4?\ C\ 1(83)}$
17	1670vs	1665w	1853	1797	97.43	0.09	1770	1682	100.00	0.78	$\nu_{O13?\ C\ 12(80)}$
18			1702	1651	0.01	0.09	1647	1596	0.03	7.34	$\nu_{CC\ (59)\ Ph\ II} + \delta_{HCC(17)\ Ph\ II}$
19			1690	1640	0.45	0.10	1641	1590	0.74	4.58	$\nu_{CC\ (65)\ Ph\ I} + \delta_{HCC(16)\ Ph\ I}$
20			1678	1628	0.08	0.11	1628	1577	0.59	1.39	$\nu_{CC\ (68)\ Ph\ I}$
21		1605w	1678	1628	0.46	0.11	1626	1576	0.10	1.29	$\nu_{CC\ (56)\ Ph\ II}$
22		1499w	1560	1513	88.33	0.11	1532	1484	64.57	0.83	$\nu_{N2C12\ (10)} + \delta_{H22N2C3(19)} + \delta_{HCC(30)\ Ph\ II}$
23			1553	1506	100.00	0.13	1527	1479	59.95	0.25	$\nu_{N2C\ 3(11)} + \delta_{H22N2C12(23)} + \delta_{HCC(26)\ Ph\ II}$
24			1542	1496	1.72	0.14	1525	1477	7.00	0.07	$\delta_{HCC(57)\ Ph\ I}$
25			1514	1469	10.34	0.14	1509	1462	17.09	0.88	$\delta_{sciHCH(72)\ CH2} + \tau_{H30C15O14C12\ (12)}$
26	1448w	1443w	1508	1463	2.63	0.14	1486	1440	1.40	0.11	$\nu_{CC\ (16)\ Ph\ I} + \delta_{HCC(43)\ Ph\ I} + \delta_{CCC(12)\ Ph\ I}$
27	1398w		1502	1457	2.09	0.17	1484	1438	1.73	0.14	$\nu_{CC\ (18)\ Ph\ II} + \delta_{HCC(53)\ Ph\ II} + \delta_{CCC(15)\ Ph\ II}$
28		1378w	1425	1382	38.91	0.18	1408	1364	2.09	2.04	$\tau_{HCOC\ (58)} + \delta_{wagHCH(42)\ CH2}$
29			1398	1356	57.23	0.18	1383	1339	36.37	1.09	$\delta_{HCC(10)} + \tau_{H23C3C1O\ 5(40)}$
30			1375	1333	6.85	0.18	1373	1330	33.17	0.76	$\delta_{H24O5C1(20)} + \delta_{H23C3C1(13)}$
31			1355	1315	0.24	0.19	1358	1316	0.18	0.09	$\delta_{HCC(79)\ Ph\ II}$
32			1350	1310	0.44	0.20	1351	1309	0.96	0.15	$\nu_{CC\ (37)\ Ph\ I}$
33	1296w		1350	1309	0.14	0.20	1342	1300	0.14	0.31	$\nu_{CC\ (77)\ Ph\ II} + \delta_{HCC(12)\ Ph\ II} + \delta_{twistHCH(12)\ CH2}$
34		1274vw	1317	1278	34.60	0.21	1312	1271	11.60	0.25	$\nu_{CC\ (25)\ Ph\ I} + \delta_{H24O5C1(12)} + \tau_{H23C3C1O5\ (19)}$
35	1246s	1248vw	1275	1237	88.04	0.22	1259	1220	55.39	1.38	$\delta_{H24O5C1(16)} + \delta_{H23C3C6(32)}$
36		1212vw	1257	1220	0.16	0.22	1251	1212	1.04	0.53	$\delta_{H31C15O14(75)}$
37			1247	1210	4.36	0.23	1238	1199	1.11	7.79	$\nu_{C15C16\ (50)} + \delta_{HCC(16)\ Ph\ II} + \delta_{CCC(12)\ Ph\ II}$
38			1246	1209	5.28	0.24	1231	1192	57.87	1.08	$\nu_{N2C12\ (21)} + \delta_{H22N2C12(22)}$
39			1238	1201	14.25	0.25	1214	1176	28.81	3.84	$\nu_{N2C\ 3(11)} + \nu_{C3C6\ (24)}$
40			1205	1169	0.62	0.25	1205	1167	0.32	1.11	$\nu_{CC\ (18)\ Ph\ I} + \delta_{HCC(65)\ Ph\ I}$
41	1165vw	1156vw	1200	1164	0.33	0.26	1202	1164	1.93	1.07	$\nu_{CC\ (23)\ Ph\ II} + \delta_{HCC(73)\ Ph\ II}$
42			1188	1152	1.11	0.28	1183	1146	0.00	0.77	$\nu_{CC\ (11)\ Ph\ I} + \delta_{HCC(79)\ Ph\ I}$
43			1183	1148	0.01	0.28	1183	1146	0.00	0.77	$\delta_{HCC(78)\ Ph\ II}$
44			1181	1146	38.67	0.29	1167	1131	29.89	1.05	$\nu_{N2C3\ (31)}$
45			1173	1138	1.38	0.29	1158	1122	19.78	0.53	$\nu_{O5C\ 1(50)} + \delta_{H24O5C1(18)}$
46		1081vw	1121	1087	0.78	0.30	1109	1074	1.09	0.09	$\nu_{CC\ (10)\ Ph\ II} + \delta_{HCC(39)\ Ph\ II}$
47	1055w		1111	1078	8.76	0.31	1104	1069	4.49	0.29	$\nu_{CC\ (39)\ Ph\ I} + \delta_{HCC(17)\ Ph\ I}$
48		1031vw	1086	1053	69.22	0.31	1057	1024	54.62	2.68	$\nu_{N2C\ 12(37)}$

49			1067	1035	2.71	0.32	1050	1017	1.40	9.00	$\nu_{CC\ (23)\ Ph\ II} + \delta_{HCC(15)\ Ph\ II} + \delta_{CCC(28)\ Ph\ II}$
50	1003w		1062	1030	3.00	0.35	1047	1014	25.58	0.53	$\nu_{CC\ (26)\ Ph\ I} + \nu_{N2C\ 3(11)} + \delta_{CCC(13)\ Ph\ I}$
51			1027	997	7.39	0.37	1019	987	0.10	14.00	$\nu_{CC\ (41)\ Ph\ I} + \delta_{CCC(45)\ Ph\ II}$
52			1019	989	1.18	0.38	1018	987	0.20	9.68	$\nu_{CC\ (30)\ Ph\ II} + \delta_{CCC(46)\ Ph\ I}$
53			1018	988	0.96	0.40	1007	976	0.24	0.11	$\tau_{HCCH\ (79)\ Ph\ I}$
54		1002vw	1017	986	0.73	0.41	1006	975	0.18	0.54	$\tau_{HCCH\ (84)\ Ph\ II}$
55			1016	986	0.90	0.41	993	962	17.17	13.13	$\nu_{O14C15\ (47)}$
56			993	963	0.04	0.42	987	956	0.22	0.18	$\gamma_{HCCC\ (74)\ Ph\ I} + \gamma_{CCCC(10)\ Ph\ I}$
57			991	962	0.09	0.47	986	955	0.01	0.01	$\gamma_{HCCC\ (79)\ Ph\ II}$
58			975	946	0.69	0.47	977	947	1.06	0.32	$\gamma_{C3C1O5H24(62)}$
59		926vw	967	938	1.56	0.47	954	924	2.26	1.45	$\nu_{CC\ (11)\ Ph\ I} + \gamma_{HCCC\ (28)\ Ph\ I}$
60			940	912	2.86	0.47	930	901	4.50	1.36	$\gamma_{HCCC\ (60)\ Ph\ II}$
61	874vw	897vw	925	898	0.41	0.48	913	884	1.13	2.56	$\nu_{CC\ (13)\ Ph\ II} + \gamma_{HCCC\ (39)\ Ph\ II}$
62		859vw	879	853	1.31	0.49	868	841	1.02	1.80	$\nu_{C3C6(11)} + \delta_{C6C3N2(11)} + \delta_{CCC(15)\ Ph\ I} + \gamma_{O13C12O14C15(17)}$
63			868	842	0.99	0.50	856	830	0.03	0.18	$\gamma_{HCCC\ (91)\ Ph\ II}$
64			868	842	0.11	0.51	855	829	0.14	0.29	$\gamma_{HCCC\ (86)\ Ph\ I}$
65	806vw	803vw	867	841	0.61	0.51	854	828	2.83	4.82	$\nu_{C15C\ 16(14)} + \delta_{CCC(22)\ Ph\ II}$
66		762vw	788	764	5.66	0.52	784	759	4.06	0.28	$\gamma_{O13N2O14C12(87)}$
67			782	759	4.94	0.53	775	751	8.07	3.08	$\gamma_{HCCC\ (12)\ Ph\ I} + \gamma_{HCCC\ (11)\ Ph\ II}$
68			777	754	3.62	0.55	770	746	3.49	0.31	$\gamma_{HCCC\ (35)\ Ph\ I} + \gamma_{CCCC(17)\ Ph\ II}$
69		720vw	751	728	2.60	0.63	740	717	4.23	0.61	$\delta_{O13C12O14(33)} + \gamma_{HCCC\ (12)\ Ph\ II}$
70	713m		740	718	15.21	0.63	734	711	11.96	2.42	$\gamma_{HCCC\ (10))\ Ph\ I} + \gamma_{O4C1O5C3(23)}$
71			713	692	4.34	0.64	709	687	1.04	0.05	$\gamma_{HCCC\ (49)\ Ph\ I} + \gamma_{HCCC\ (11)\ Ph\ II} + \gamma_{CCCC(19)\ Ph\ I}$
72			712	691	14.61	0.68	708	686	21.77	0.02	$\gamma_{HCCC\ (17)\ Ph\ I} + \gamma_{HCCC\ (18)\ Ph\ II} + \gamma_{CCCC(22)\ Ph\ II}$
73	644w	651vw	667	647	8.21	0.69	658	637	5.40	0.42	$\delta_{O5C1O4(48)}$
74			637	618	21.21	0.71	636	616	0.36	2.53	$\delta_{CCC(82)\ Ph\ II}$
75			632	613	0.53	0.76	633	613	14.97	1.56	$\delta_{O4C1O5(56)}$
76			630	611	19.04	0.79	629	610	4.96	2.12	$\delta_{CCC(76)\ Ph\ I}$
77		616vw	623	604	7.65	0.80	614	594	21.83	2.28	$\delta_{N2C12O14(23)} + \tau_{O5H24C1C3\ (47)}$
78	563w	556vw	584	567	3.50	0.82	582	564	3.36	0.22	$\delta_{O13C12O14(12)} + \delta_{CCC(40)\ Ph\ II}$
79			548	532	2.64	0.83	542	525	3.98	0.76	$\delta_{N2C12O14(17)} + \tau_{O5H24C1C\ 3(18)} + \gamma_{CCCC(14)\ Ph\ II}$
80	496w		505	490	5.21	0.84	500	484	6.03	0.97	$\tau_{O5H24C1C3\ (12)} + \gamma_{CCCC(29)\ Ph\ I}$
82		465vw	494	479	12.47	0.85	487	472	9.40	0.70	$\gamma_{H22N2C12O13(56)}$
83			491	476	16.02	0.86	413	400	0.01	0.01	$\tau_{HCCC\ (11)\ Ph\ II} + \gamma_{CCCC(80)\ Ph\ II}$
84			417	404	0.03	0.91	411	398	0.13	0.04	$\tau_{HCCC\ (12)\ Ph\ I} + \gamma_{CCCC(79)\ Ph\ I}$
85		375vw	414	402	0.17	0.95	376	365	0.64	1.52	$\delta_{C3C1O5(57)}$
86			381	369	0.80	0.98	348	337	0.18	1.50	$\delta_{C6C3N2(26)} + \gamma_{CCCC(14)\ Ph\ II}$
87			351	341	0.25	1.01	331	320	0.25	0.16	$\delta_{CCC(77)\ Ph\ II}$
88		307w	325	315	0.17	1.21	313	303	0.22	0.78	$\nu_{CC\ (13)\ Ph\ I} + \delta_{C1C3N2(33)}$
89		273w	316	307	0.27	1.41	255	247	3.76	2.90	$\delta_{C15O14C12(52)}$
90		222w	257	249	4.24	1.54	228	221	1.43	2.38	$\delta_{C12N2C3(17)} + \gamma_{CCCC(11)\ Ph\ II}$
91			232	225	1.60	2.04	207	200	0.02	4.82	$\delta_{C6C3N2(11)} + \gamma_{CCCC(12)\ Ph\ I} + \gamma_{C6C3N2C12(24)}$
92			208	202	0.08	2.37	192	186	1.54	3.86	$\delta_{C6C3N2(55)}$
93		122w	195	189	1.50	2.41	125	122	0.12	1.35	$\tau_{C15O14C12N2\ (64)}$
94			137	133	0.13	2.63	112	109	0.32	6.40	$\delta_{C12N2C(340)} + \gamma_{CCCC(21)\ Ph\ II}$
95		78w	118	114	0.42	2.73	85	83	0.15	14.75	$\gamma_{C6C3N2C12(79)}$
96			94	91	0.54	2.74	71	69	1.61	1.73	$\tau_{C3N2C12O13(69)} + \tau_{N2C3C1O5(12)}$
97			85	83	1.05	2.79	52	50	0.31	13.59	$\tau_{C3N2C12O13(11)} + \tau_{N2C3C1O4(75)}$
98			72	70	0.49	3.89	46	44	0.20	36.79	$\delta_{C3C1O5(51)} + \gamma_{CCCC(24)\ Ph\ II}$
99			52	51	0.20	10.42	26	25	0.01	90.37	$\gamma_{C6C3N2C12(77)}$
100			38	37	0.07	10.71	24	24	0.05	100.00	$\tau_{C11C6C3N2\ (88)}$
101			22	21	0.04	32.94	16	16	0.02	67.91	$\tau_{C3N2C12O14(72)}$
102			12	12	0.01	100.00	12	11	0.02	65.34	$\tau_{C3N2C12O13\ (85)}$

ν stretching; δ in-plane bending; γ out-of-plane bending; τ torsion; ρ rocking; w-weak; s-strong; vs-very strong; vw-very weak. [a]I_{IR}-IR Intensity ($Kmmol^{-1}$). [b]I_{Ra}-Raman intensity (Arb units) (intensity normalized to 100 %).

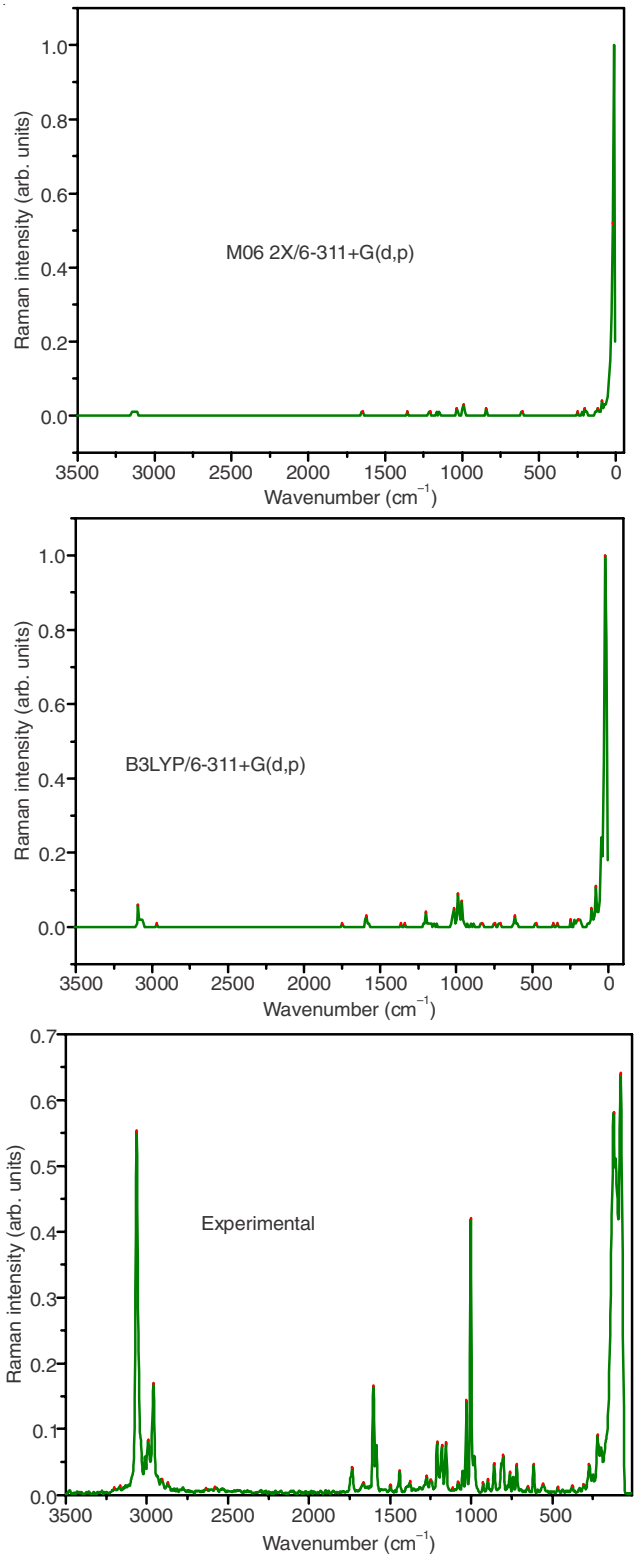

Fig. 4. Comparison of theoretical M06 2X/6-311+G (d,p) and B3LYP/6-311+G (d,p) and experimental FT-Raman spectra for N-carbobenzoxy-L-2-phenylglycine

the fundamental vibrations are observed in both IR and Raman complementarily. All the calculated normal modes are numbered from the largest to the smallest frequency within each fundamental wavenumber.

The potential energy distribution (PED) for each normal mode among the symmetry coordinates of the molecules was calculated. Root mean square (RMS) values were obtained in the study using the following expression:

$$\sqrt{\frac{1}{n-1}\sum_{i}^{n}\left(\nu_{i}^{cal}-\nu_{n}^{exp}\right)^{2}}$$

where, 'n' is the number of the experimental or calculated data. The RMS error was calculated between scaled M06-2X/6-311+G(d,p) and B3LYP/6-311+G(d,p) and experimental frequencies. This is quite obvious since the frequencies calculated on the basis of quantum mechanical force fields usually differ appreciably from observed frequencies. This is partly due to the neglect of anharmonicity and partly due to the approximate nature of the quantum mechanical methods. In order to reproduce the observed frequencies, refinement of scaling factors were applied and optimized *via* least square refinement algorithm which resulted in a weighted RMS deviation of the observed IR and Raman bands are found to be 6.79 and 4.65 by M06-2X and 3.65 and 2.71 by B3LYP methods, respectively. The small differences between experimental and calculated vibrational modes are observed. It must be due to the fact that hydrogen bond vibrations present in the crystal lead to strong perturbation of the IR wavenumbers and intensities of many other modes.

Vibrations of the phenyl rings: The aromatic structures show the presence of C–H stretching vibrations in the region 3100-3000 cm^{-1}. In this region, the groups are not influenced considerably by the way of substituent [51]. Five aromatic C–H stretching modes for each phenyl ring I and II (mode numbers 3-12) are expected in the region of 3032-3001 cm^{-1} by B3LYP and 3145-3110 cm^{-1} by M06-2X method, respectively for the vibrational spectra of CbzLPG. These modes are observed at 3039 cm^{-1} in FTIR spectra and at 3063 and 2992 cm^{-1} in FT-Raman spectra. The modes (3-12) are due to C–H stretching of hydrogen bonded carbon atoms of phenyl rings. These modes are pure C–H stretching vibrations with a PED contribution nearly 90 %. Five in-plane C–H deformation modes are usually observed for mono substituted benzenes in the following frequency intervals: 1331-1253, 1184-1176, 1165-1147 and 1032-1019 and 1082-1065 cm^{-1} [11]. In our present study C–H in-plane deformation vibrations of the phenyl rings observed at 1398 cm^{-1} in FTIR spectra and at 1499 and 1443 cm^{-1} in FT-Raman spectra. The computed scaled wavenumbers at 1651, 1640, 1513, 1506, 1496, 1463, 1457, 1315, 1169 and 1152 cm^{-1} by M06-2X level of calculation and at 1596, 1590, 1484, 1479, 1477, 1440, 1438, 1316, 1167 and 1146 cm^{-1} by B3LYP level of calculation. The observed picture in this spectral range is consistent with the B3LYP theoretical predictions for the CbzLPG. The C–H out-of-plane bending vibrations occur to the range 1000-750 cm^{-1} in the aromatic compounds [51]. In our case C-H out-of plane bending vibrations of the phenyl rings observed at 874 and 713 cm^{-1} in FTIR spectra and at 926, 897 and 720 cm^{-1} in FT-Raman spectra. Theoretically C–H out-of plane bending vibrations are assigned to the wavenumber range 963-962, 938-898, 842, 759 and 718-691 cm^{-1} by M06-2X level of calculation and 956-955, 924-884, 830, 751 and 711-686 cm^{-1} by B3LYP level of calculation. These observed results are in good agreement with the DFT calculations performed for the model CbzLPG system.

Five normal modes derived from the aromatic C–C stretching modes are expected in the vibrational spectra of mono substituted benzene derivatives in the following regions: 1614–1575 cm^{-1}, 1515–1440 cm^{-1} and 1350–1300 cm^{-1} [11]. In the present work, the wavenumbers observed at 1448, 1398, 1296 and 1165 cm^{-1} in the IR spectrum, 1605, 1443, 1274, 1156 and 1081 cm^{-1} in the Raman spectrum and computed wavenumbers at 1640-1628, 1463-1457, 1310-1278, 1164 and 1087 cm^{-1} by M06-2X and 1641-1626, 1440-1438, 1309-1271, 1164 and 1074 cm^{-1} by B3LYP level of calculation are assigned as C–C stretching modes of phenyl rings. The PED % values corresponding to all the C-C vibrations lie between 10 and 65 % as shown in Table-2. The in-plane ring deformation/skeletal C-C-C vibrations always occurs between the values 1000-600 cm^{-1} for mono substituted benzenes [52]. In the present investigation the wavenumbers observed in IR/Raman spectra at 1003/859, 806/803 cm^{-1} has been assigned to C-C-C in-plane ring deformation. The theoretical computed values in M06-2X/B3LYP at 1035/1017, 1030/1014, 997/987, 989/987, 853/841, 841/828, 618/616, 611/610 cm^{-1} are identified as C-C-C in-plane ring deformation. The C–C–C out off plane bending vibrations observed the weak bands at 496 cm^{-1} in IR and 222 cm^{-1} in FT-Raman spectrum. The theoretically predicted wave numbers in M06-2X/B3LYP at 963/956, 754/746, 692/687, 691/686, 490/484 and 249/221 cm^{-1} are assigned as C–C–C out off plane bending vibrations, this is good agreement with experimental findings.

Vibrations of the carboxylic group: Vibrational analysis of -COOH group is significant because the drug activity of the title compound is mainly due to the presence of this moiety. Vibrational analysis of carboxylic acid is made on the basis of carbonyl group, carboxyl group and hydroxyl group. The C=O stretching from carboxylic acids is identical to the C=O stretching of ketones, which is expected in the region 1740–1660 cm^{-1}. In CbzLPG the C1=O4 is observed at 1739 cm^{-1} as a medium band in IR and 1734 cm^{-1} in Raman spectrum. The computed wavenumber at 1837 cm^{-1} by M06-2X and 1715 cm^{-1} by B3LYP have been assigned to C1=O4 stretching mode. This is a pure mode the contribution of PED is 83 % shown in Table-2. Govindarasu and Kavitha [53] identified calculated wavenumber at 1387 cm^{-1} was identified C–O stretching vibration coupled with COH in plane bending vibration in carboxyl group. In our present work the computed wavenumber at 1138 cm^{-1} by M06-2X and 1122 cm^{-1} by B3LYP have been identified as C–O stretching vibration coupled with COH in plane bending vibration. The C=O in-plane deformation is weakly to moderately active in the region 725 ± 95 cm^{-1}. Most carboxylic acids display γ(C=O) in the region 595 ± 85 cm^{-1} which is in the vicinity of that of methyl and ethyl esters [54]. The observed frequency at 644 cm^{-1} in FT-IR spectrum and 651 cm^{-1} in FT-Raman spectrum observed as OC=O in plane bending vibrations. This band was calculated at 647 cm^{-1} by M06-2X and 637 cm^{-1} by B3LYP level of calculation. The observed medium band at 713 cm^{-1} in FTIR spectrum and computed wavenumber at 718 cm^{-1} by M06-2X and 711 cm^{-1} by B3LYP level of calculation have been identified as OC=O out-of-plane bending vibration.

The hydroxyl stretching vibrations are generally observed in the region 3600–3400 cm^{-1} [55]. The medium band observed at 3652 cm^{-1} in IR is assigned to OH stretching mode of the

TABLE-2
SECOND ORDER PERTURBATION THEORY ANALYSIS OF FOCK MATRIX IN NBO BASIS FOR N-CARBOBENZOXY-L-2-PHENYLGLYCINE

Donor (i)	E_D (i) (e)	Acceptor (j)	E_D (j) (e)	E(2)[a] (KJ mol^{-1})	E(j)-E(i)[b] (a.u)	F(i,j)[c] (a.u)
π(C6-C11)	1.659	π*(C7-C5)	0.321	20.36	0.28	0.068
		π*(C9-C10)	0.327	20.00	0.28	0.067
π(C7-C8)	1.664	π*(C6-C11)	0.348	20.84	0.29	0.069
		π*(C9-C10)	0.326	20.26	0.28	0.068
π(C9-C10)	1.661	π*(C6-C11)	0.348	20.58	0.29	0.069
		π*(C7-C8)	0.321	20.14	0.28	0.068
π(C16-C17)	1.974	π*(C18-C19)	0.328	20.27	0.28	0.068
		π*(C20-C21)	0.319	20.39	0.28	0.068
π(C18-C19)	1.660	π*(C16-C17)	0.347	20.50	0.29	0.069
		π*(C20-C21)	0.319	19.77	0.28	0.067
π(C20-C21)	1.661	π*(C16-C17)	0.347	20.66	0.29	0.069
		π*(C18-C19)	0.328	20.60	0.28	0.068
LP(1) N2	1.744	σ*(C12-O13)	0.174	13.68	0.61	0.083
		π*(C12-O13)	0.210	15.01	0.54	0.081
LP(2) O4	1.846	σ*(C1-C3)	0.074	18.75	0.63	0.099
		σ*(C1-O5)	0.092	32.23	0.63	0.129
LP(2) O5	1.818	π*(C1-O4)	0.209	46.17	0.35	0.114
LP(1) O13	1.978	RY*(1) C12	0.019	17.26	1.83	0.159
LP(2) O13	1.836	σ*(N2-C12)	0.068	22.05	0.72	0.115
		σ*(C12-O14)	0.099	31.08	0.61	0.125
LP(2) O14	1.830	π*(C12-O13)	0.210	13.59	0.60	0.081
σ*(C12-O13)	0.174	σ*(C12-O14)	0.099	12.67	0.02	0.034
π*(C12-O13)	0.210	π*(C12-O13)	0.174	294.08	0.07	0.295

E_D means electron density; [a]E(2) means energy of hyper conjugative interactions; [b]Energy difference between donor and acceptor i and j NBO orbitals; [c]F(i,j) is the Fock matrix element between i and j NBO orbitals

carboxylic acid which is calculated at 3718 and 3639 cm^{-1} by M06-2X and B3LYP level of calculation, respectively. The OH in plane bending gives rise to a strong band in the region 1440–1260 cm^{-1} [55]. The strong band at 1246 (IR) and 1248 (Raman) cm^{-1} and 1237 cm^{-1} (M06-2X) and 1220 cm^{-1} (B3LYP) correspond to the OH in plane bending mode. The OH out-of-plane bending vibration gives rise to a band in the region 700–600 cm^{-1}. In the present study CCOH torisional band observed at 616 cm^{-1} in FT-Raman spectrum. The computed wavenumber at 604 cm^{-1} and 594 cm^{-1} by M06-2X and B3LYP, respectively were assigned CCOH torisional bending vibration.

Vibrations of the methylene group: The methylene group vibrations are assigned to the basis of the spectral similarity with the related amino acid compounds. In amino acids, the CH_2 asymmetric and symmetric stretching vibrations are expected to occur in the regions 3100–3000 and 3000–2900 cm^{-1}, respectively [56]. Vibrations computed by the M06-2X/B3LYP level of calculations were at 3076/2952cm^{-1} and 3022/2907 cm^{-1} (mode no's 13 and 15) and were assigned to CH_2 asymmetric and symmetric stretching modes of CH_2 unit. The bands at 2964 cm^{-1} in FT-IR and 2961 cm^{-1} in FT-Raman spectrum were assigned to CH_2 antisymmetric stretching vibrations. This is correlates well with computed values. The CH_2 bending modes follow, in decreasing wavenumber, the general order CH_2 deformation > CH_2 wagging > CH_2 twist > CH_2 rock. The CH_2 scissoring vibrations appear normally in the region 1490–1435 cm^{-1} as medium intense bands [56]. In present study the theoretically predicted wavenumber at 1469 cm^{-1} (M06-2X) and 1462 cm^{-1} B3LYP have been assigned CH_2 scissoring vibration (mode no. 25), which evident from the PED column almost contributes to 72 %. Absorption of hydrocarbons due to CH_2 twisting and wagging vibration is observed in the 1350–1150 cm^{-1} region [57]. These bands are generally appreciably weaker than those resulting from CH_2 scissoring vibration. In our title molecule the observed band at 1296 cm^{-1} in FTIR and 1378 cm^{-1} in FT-Raman spectrum and computed wavenumber in M06-2X/B3LYP at 1382/1364 cm^{-1} and 1309/1300 cm^{-1} were identified as CH_2 wagging and twisting vibrations, respectively.

Vibrations of carbonyl group: The carbonyl stretching C=O vibrations [51] are expected in the region 1715–1680 cm^{-1} and in the present study this mode appears at 1670 cm^{-1} in the IR spectrum as a strong band and at 1665 cm^{-1} in the Raman spectrum as a weak band. The M06-2X/B3LYP calculations give this mode at 1797/1682 cm^{-1}. The C=O in-plane bending vibrations are observed at 563 cm^{-1} in FTIR spectrum and 720 and 556 cm^{-1} in FT-Raman spectrum and theoretically predicted wavenumbers in M06-2X/B3LYP level of calculations at 728/717 cm^{-1} and 567/564 cm^{-1} have been assigned as C=O in-plane bending vibrations. The out-of-plane C=O vibrations identified with 859 cm^{-1} in FT-Raman spectrum and 853 cm^{-1} by M06-2X and 841 ccm^{-1} by B3LYP level of calculations.

Vibrations of NH and CH group: The N–H stretching vibrations generally give rise to bands at 3500–3300 cm^{-1} [58]. In the present case, the bands calculated at 3570 cm^{-1} (M06-2X) and 3363 cm^{-1} (B3LYP) assigned as NH stretching vibrations. Furthermore observed NH stretching frequency 3402 cm^{-1} in the IR spectrum with a strong intensity is shifted by 168 cm^{-1} and 39 cm^{-1} from the computed value 3570 cm^{-1} (M06-2X) and 3363 cm^{-1} (B3LYP), respectively, this frequency difference may be due to N–H···O inter molecular interactions of NH and carboxyl group of the title compound. Panicker *et al*. [59] reported NH deformation bands at 1538, 1220 cm^{-1} in IR spectrum and at 1538 and 1223 cm^{-1} theoretically. In our present investigations NH in-plane bending δ(CNH) vibration is observed at 1499 cm^{-1} (Raman) and computed wavenumbers at 1513/1484 cm^{-1} and 1506/1479 cm^{-1} by M06-2X/B3LYP level of calculations, this is good agreement with experimental findings. Mode no: 82 have been identified as NH out-of-plane vibrations of the title compound.

The C3-H23 stretching vibrations theoretically predicted at 3046 cm^{-1} by M06-2X and 2925 cm^{-1} by B3LYP level of calculations. The C1C3H23 and C6C3H23 in-plane bending vibrations are identified at 1333 cm^{-1} by M06-2X and 1330 cm^{-1} by B3LYP (mode no. 30) and 1237 cm^{-1} by M06-2X and 1220 cm^{-1} by B3LYP level of calculations, respectively and 1246/1248 cm^{-1} (IR/Raman, mode no. 31). The Mode no: 34 have been identified as C3-H23 torsion vibration of the title compound.

Analysis of vibrational calculations: The correlation image which often talks about tranquility relating to the calculated as well as experimental numbers. As seen from the Fig. 5, the experimental fundamental has a good correlation with B3LYP level. The relations relating to the calculated and experimental wave numbers are linear and identified by the using equations:

$$\nu_{cal} = 1.019\ \nu_{exp} + 3.771;\ (R^2 = 0.998) \text{ at DFT/M06-2X level}$$

$$\nu_{cal} = 1.003\ \nu_{exp} + 3.623;\ (R^2 = 0.999) \text{ at DFT/B3LYP level}$$

We calculated R^2 values (R^2 = 0.999 for B3LYP and R^2 = 0.998 for M06-2X) between the calculated and experimental wavenumbers. As a result, the performances of the B3LYP method with the prediction of the wavenumbers within the molecule were quite close.

NBO analysis and static polarizability and first order hyperpolarizability analysis: Natural bond orbital (NBO) analysis provides the most accurate possible 'natural Lewis structure' picture of, because the many orbital particulars are mathematically selected to include highest possible percentages of the electron density. A convenient aspect of NBO technique is that gives information all about interactions within both stuffed and also virtual orbital spaces. This could enhance ones analysis associated with intra as well as inter-molecular interactions. The second order Fock matrix is performed to check on the donor-acceptor interactions with the NBO analysis [60]. The interactions result is a loss of the occupancy from the localized NBO of an idealized Lewis structure into an empty non-Lewis orbital. For each donor (i) and acceptor (j), the stabilization energy $E^{(2)}$ associated with the delocalization i→j is estimated as

$$E_2 = \Delta E_{ij} = q_i \frac{F(i,j)^2}{\varepsilon_j - \varepsilon_i}$$

where q_i is the donor orbital occupancy, are ε_i and ε_j diagonal elements and F(i, j) is the off diagonal NBO Fock matrix element.

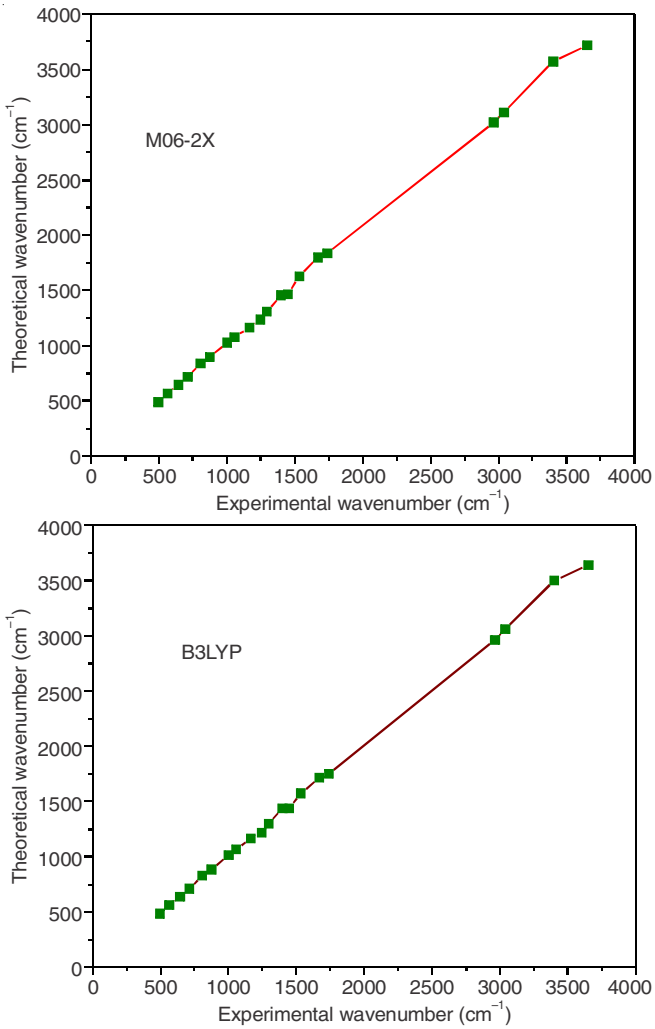

Fig. 5. Correlation graphs of experimental and theoretical (scaled) wavenumbers of the N-Carbobenzoxy-L-2-phenylglycine

The natural bond orbital calculation was carried out utilizing NBO 3.1 program implemented in the Gaussian 09 [30] package at the DFT/B3LYP level of calculation order to appreciate quite a lot of second-order interactions between the filled orbitals of one subsystem and vacant orbitals of an another subsystem, which is measuring the designated delocalization or hyper conjugation. In Table-2, the perturbation energies of significant donor–acceptor interactions were presented. The larger the $E^{(2)}$ value, intensive would be the interaction between electron donors and also electron acceptors. The intramolecular interactions are generally created with the orbital overlap in between σ(C–C), σ*(C–C), π(C–C) and π*(C–C) bond orbital which results intramolecular charge transfer (ICT) causing stabilization of the system. These interactions are seen as increases in electron density in C–C antibonding orbital that weakens the respective bonds.

The strong intramolecular hyper conjugation interaction of the σ and π electron of C–C, C–H, C–N and C–O to the anti C–C, C–H and C–N bond leads to stabilization of some part of the ring (Table-2). The intramolecular hyperconjugative interaction of the π(C6-C11) distributes to π*(C7-C5), π*(C9-C10), leads to less stabilization of 20.36 kJ/mol and 20.00 kJ/Mol, respectively. This enhanced further conjugate with bonding orbital of π (C7-C8) π*(C6-C11) and π*(C9-C10) which leads to strong delocalization of 20.84 and 20.26 kJ/mol, respectively. The σ*(C12-O13) of the NBO conjugated with σ*(C12-O14) resulting to stabilization of 12.67 kJ/mol. Other intramolecular hyperconjucative interactions were presented in Table-2.

Hyperpolarizabilities are very sensitive to the basis sets and levels of theoretical approach employed [61,62], that the electron correlation can change the value of hyperpolarizability. It is already established that the molecular hyperpolarizability and mechanical stabilities get enhanced in organic molecules containing O–H and N–H groups, which involved in hydrogen bond interactions [63]. Urea is one of the prototypical molecules utilized as a part of the investigation of the non-linear optical (NLO) properties of molecular frameworks. Thus it's been used frequently being a threshold code for comparative purposes.

The first static hyperpolarizability (β_o) and its related properties (β, α_o and Δα) have been computed utilizing B3LYP/6-311+G(d,p) level taking into account on finite field approaches. In the presence of a utilized electric field, the energy of a system is a function of the electrical field and hyperpolarizability is a third rank tensor that can be depicted by a 3 × 3 × 3 network. The 27 parts of the 3D framework can be lessened to segments as a result of the Kleinman symmetry [44]. The matrix can be given in the lower tetrahedral format. It is obvious that the lower part of the 3 × 3 × 3 matrices is a tetrahedral. The components of β are defined as the coefficients in the Taylor series expansion of the energy in the external electric field. When the external electric field is weak and homogeneous, this expansion is given below:

$$E=E^{\circ} - \mu_{\alpha}F_{\alpha} - 1/2\ \alpha_{\alpha\beta}F_{\alpha}F_{\beta} - 1/6\ \beta_{\alpha\beta\gamma}F_{\alpha}F_{\beta}F_{\gamma+.....}$$

where E^{o} is the energy of the unperturbed molecules, F_{α} is the field at the origin, μ_{α}, $\alpha_{\alpha\beta}$ and $\beta_{\alpha\beta\gamma}$ are the components of dipole moment, polarizability and first hyperpolarizability, respectively.

The total static dipole moment (μ), the mean polarizability (α_o), the anisotropy of the polarizability (Δα) and the mean first hyperpolarizability (β_o), using the x, y and z components are defined as:

Dipole moment is:

$$\mu = (\mu^2_x + \mu^2_y + \mu^2_z)^{1/2}$$

Static polarizability is:

$$\alpha_0 = (\alpha_{xx} + \alpha_{yy} + \alpha_{zz})/3$$

Total polarizability is:

$$\Delta\alpha = 2^{-1/2}[(\alpha_{xx}-\alpha_{yy})^2 + (\alpha_{yy}-\alpha_{zz})_2 + (\alpha_{zz}-\alpha_{xx})^2 + 6\alpha^2_{xz}]^{1/2}$$

First order hyperpolarizability is:

$$\beta = (\beta^2_x + \beta^2_y + \beta^2_z)^{1/2}$$

where:

$$\beta_x = (\beta_{xxx} + \beta_{xyy} + \beta_{xzz})$$

$$\beta_y = (\beta_{yyy} + \beta_{yzz} + \beta_{yxx})$$

$$\beta_z = (\beta_{zzz} + \beta_{zxx} + \beta_{zyy})$$

$$\beta = [(\beta_{xxx} + \beta_{xyy} + \beta_{xzz})^2 + (\beta_{yyy} + \beta_{yzz} + \beta_{yxx})^2 + (\beta_{zzz} + \beta_{zxx} + \beta_{zyy})^2]^{1/2}$$

Since the values of the polarizabilities (α) and hyperpolarizability (β) of the Gaussian 09 output are reported in

atomic units (a.u.), the calculated values have been converted into electrostatic units (esu) (For α: 1a.u. = 0.1482 × 10^{-24} esu; For β: 1a.u. = 8.639 × 10^{-33} esu). The mean polarizability α_o and total polarizability Δα of our title molecule are 30.4228 × 10^{-24} esu and 4.3256 × 10^{-24} esu, respectively. The total molecular dipole moment and first order hyperpolarizability are 0.4691 Debye and 475.0223 × 10^{-33} esu, respectively and are depicted in Table-3. The first order hyperpolarizability of CbzLPG molecule is approximately 1.27 times greater than that of urea (β of urea is 372.8 × 10^{-33} esu [64]. This result indicates the good non-linearity of the title molecule.

Electronic properties

UV-visible spectral analysis: Ultraviolet spectra analyses of CbzLPG have been investigated by theoretical calculation. In order to understand electronic transitions of compound, TD-DFT calculations on electronic absorption spectra in gas phase and solvent (ethanol) are performed. The electronic absorption spectra of the title compound in ethanol solvent has been recorded within the 200–800 nm range and representative spectra are shown in Fig. 6. On the basis of fully optimized ground-state structure, TDDFT/B3LYP/6-311+G(d,p) calculations have been used to determine the low-lying excited states of CbzLPG. The theoretical and experimental maximum absorption wavelengths are compared in Table-4. As can be seen from the Table-5, TD-DFT level predicts three intense electronic transitions for both solvent and gas phase, one at 5.1682/5.1514 eV (239.90/240.68 nm), 5.2998/5.2896 eV (233.94/234.39 nm) and 5.3721/5.3488 eV (230.79/231.80 nm) with oscillator strength f = 0.0130/0.0535, 0.001/0.0006 and 0.0789/0.0094, respectively, is in good agreement with the measured experimental data in ethanol solution (exp = 223/258/252 nm). These values may be slightly shifted by solvent effects. Contrasting these qualities and the relating experimental values, TD-DFT system for both in gas stage and dissolvable media is helpful to anticipate UV-visible spectrum. Molecular orbital coefficients examination taking into account optimized geometry demons-

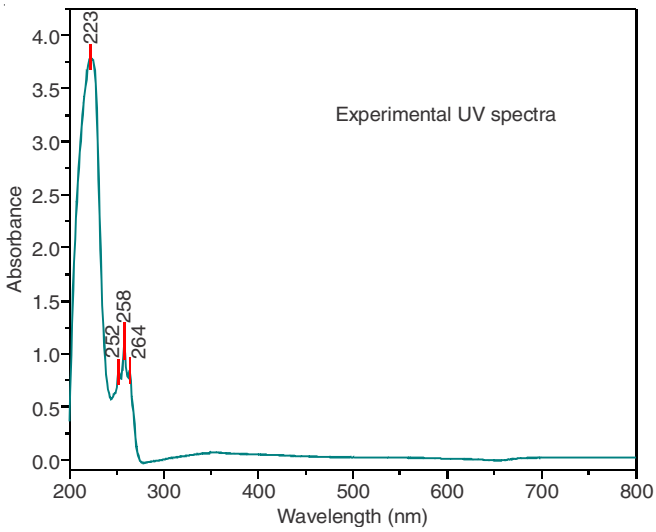

Fig. 6. UV-visible spectrum (ethanol) of N-carbobenzoxy-L-2-phenylglycine

TABLE-3
ELECTRIC DIPOLE MOMENT, POLARIZABILITY AND FIRST ORDER HYPERPOLARIZABILITY OF N-CARBOBENZOXY-L-2-PHENYLGLYCINE BY B3LYP/6-311 + G(d,p) METHOD

Dipole moment, μ (Debye)		Polarizability α			First order hyperpolarizability β		
Parameter	Value (DB)	Parameter	a.u.	esu (×10^{-24})	Parameter	a.u.	Esu (×10^{-33})
μ_x	-0.1864	α_{xx}	224.0569	33.2052	β_{xxx}	32.9565	284.711
μ_y	-0.3157	α_{xy}	-19.6172	-2.9073	β_{xxy}	-13.7257	-118.58
μ_z	-0.2913	α_{yy}	197.1311	29.2148	β_{xyy}	-11.9308	-103.07
μ	0.4691	α_{xz}	-4.2643	-0.632	β_{yyy}	-5.2336	-45.213
		α_{yz}	-4.6640	-0.6912	β_{xxz}	-83.0143	-717.16
		α_{zz}	194.6600	28.8486	β_{xyz}	16.7534	144.732
		α_o	205.2826	30.4228	β_{yyz}	9.7268	84.0301
		Δα	29.1879	4.3256	β_{xzz}	31.1279	268.914
					β_{yzz}	32.2908	278.96
					β_{zzz}	62.0753	536.269
					β_{tot}	54.9858	475.0223

TABLE-4
COMPARISON OF EXPERIMENTAL AND CALCULATED ABSORPTION WAVELENGTH (λ, nm), EXCITATION ENERGIES (E, eV) AND OSCILLATOR STRENGTH (*f*) OF N-CARBOBENZOXY-L-2-PHENYLGLYCINE

TD-DFT/ B3LYP/6-311 + G(d,p)				Experimental	
λ (nm)	E (eV)	*f* (a.u)	Major contributes	λ (nm)	Abs
Ethanol					
239.90	5.1682	0.0130	H–1→L	223	2.2315
233.94	5.2998	0.0010	H–1→L + 2 H→L + 2	258	0.1987
230.79	5.3721	0.0789	H→L	252	0.1244
				264	0.7980
Gas phase					
240.68	5.1514	0.0535	H–1→L		
234.39	5.2896	0.0006	H–1→L + 2 H→L + 2		
231.80	5.3488	0.0094	H→L		

trate that, for the title compound, frontier molecular orbitals are mainly composed of π-atomic orbitals, so the electronic transitions tend to be generally derived from contribution of bands $\pi \rightarrow \pi^*$.

Frontier molecular orbitals and global reactivity descriptors: The most imperative orbitals in a molecule are the frontier molecular orbitals (FMOs), called HOMO and LUMO and exceptionally valuable for physicists and scientists are the fundamental orbital part in chemical reaction. The HOMO energy describes the capacity of an electron giving; LUMO portrays the capacity of electron tolerating. While the HOMO's vitality is straight forwardly identified with the ionization potential, LUMO vitality is specifically identified with the electron affinity. Surfaces for the frontier orbitals were drawn to understand the bonding scheme of present compound.

Here, four important molecular orbitals (MOs) were examined: the second highest and highest occupied MOs and the lowest and the second lowest unoccupied MOs, which are denoted as HOMO-1, HOMO, LUMO and LUMO+1, respectively. The plots of highest occupied molecular orbitals (HOMOs) and lowest unoccupied molecular orbitals (LUMOs) are shown in Fig. 7. It is clear from the figure that the HOMO, HOMO-1 and LUMO+1 are located over the entire molecule and LUMO is located over the phenyl ring I. The calculated energy values of the HOMO and LUMO are 7.0381 eV and 1.0531 eV, respectively. Similarly, the HOMO-1 and LUMO+1 energy values are -0.7772 eV and -7.1391 eV, respectively. In this molecule, the value of energy separation between the HOMO and LUMO/HOMO-1 and LUMO+1 is 5.985 eV/ 6.3619 eV, respectively.

HOMO Energy -7.0381 eV
HOMO-1 Energy = -0.7772 eV
LUMO Energy = -1.0531 eV
LUMO+1 Energy = -7.1391 eV
HOMO–LUMO Energy gap = 5.985 eV
HOMO-1–LUMO+1 Energy gap = 6.3619 eV

Density functional theory is one of the important tools of quantum chemistry to understand popular chemical concepts such as electronegativity, electron affinity, chemical potential and ionization potential. The energy gap between HOMO and LUMO is a critical parameter to determine molecular electrical transport properties. By using HOMO and LUMO energy values for a molecule, the global chemical reactivity descriptor of molecules such as hardness, chemical potential, softness, electronegativity and electrophilicity index as well as local reactivity have been defined [65-69]. Pauling introduced the concept of electronegativity as the power of an atom in a molecule to attract electrons to it. Hardness (η), chemical potential (μ) and electronegativity (χ) and softness (S) are defined follows:

$$\eta = \frac{1}{2}\left(\frac{\partial zE}{\partial Nz}\right)V(r) = \frac{1}{2}\left(\frac{\partial u}{\partial N}\right)V(r)$$

$$\mu = \left(\frac{\partial E}{\partial N}\right)V(r)$$

$$\chi = -\mu - -\left(\frac{\partial E}{\partial N}\right)V(r)$$

where E and V(r) are electronic energy and external potential of an N-electron system, respectively. Softness is a property

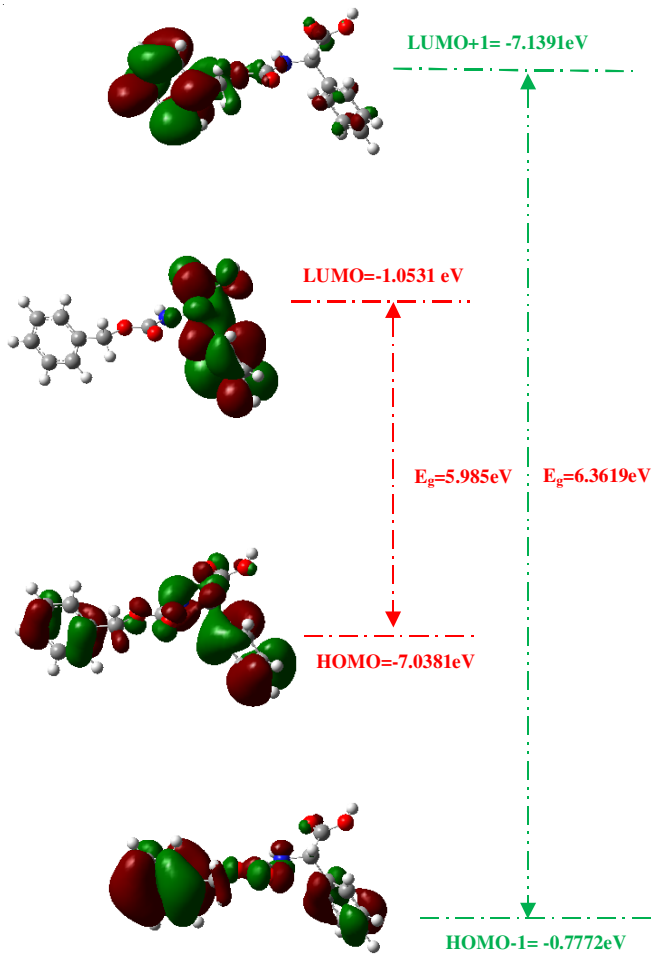

Fig. 7. Atomic orbital compositions of the frontier molecular orbital for N-carbobenzoxy-L-2-phenylglycine

of the molecule that measures the extent of chemical reactivity. It is the reciprocal of hardness:

The softness of the molecule is

$$S = 1/2\eta$$

Using Koopman's theorem [70] for closed-shell molecules, η, μ and χ can be defined as:

The hardness of the molecule is:

$$\eta = (I - A)/2$$

The chemical potential of the molecule is:

$$\mu = -(I+A)/2$$

The electronegativity of the molecule is:

$$\chi = (I + A)/2$$

The electrophilicity index of the molecule is:

$$\omega = \mu^2/2\eta$$

where I is the ionization potential and A is the electron affinity of the molecule. Electron affinity (I) and ionization potential (A) can be expressed through HOMO and LUMO orbital energies as $I = -E_{HOMO}$ and $A = -E_{LUMO}$. The ionization potential (I) and an electron affinity (A) of our molecule CbzLPG calculated by B3LYP/6-311+G(d,p) level of calculation is 1.0531 and 7.0381 eV, respectively. The calculated values of the hardness, softness, chemical potential, electronegativity and electrophilicity index of our molecule is 2.9925, 0.1670, -4.0456,

4.0456 and 2.7346, respectively. Considering the chemical hardness, large HOMO–LUMO energy gap represent a hard molecule and small HOMO–LUMO energy gap represents a soft molecule. The HOMO–LUMO energy gap of the title molecule is large 5.985 eV, so it is concluded that our molecule is hard molecule, which is evident from the calculation chemical hardness is 2.9925, which are greater than that of chemical softness 0.1670.

Molecular electrostatic potential: In the present study, molecular electrostatic potential (MEP) of our molecule CbzLPG is illustrated with Fig. 8. In the majority of the MEP, while the maximum negative region preferred a site for elctrophilic attack indications as red colour. The maximum positive region preferred a site for nucleophilic attack symptoms of blue colour. Electrostatic potential maps are very useful three dimensional diagrams of molecules. The colour code of these maps is in the range of -6.389e^{-2} a.u. (deepest red) and 6.389e^{-2} a.u. (deepest blue) in our compound, where blue indicates the strongest attraction and red indicated the repulsion. As can be seen from the MEP map of the title molecule, which regions have the negative potential are over the electro negative atoms (oxygen, nitrogen atoms) the region having the positive potential is over the hydrogen atoms.

Thermodynamic properties: Based on vibrational analysis, the statically thermodynamic functions: heat capacity ($C^{o}_{p;m}$), entropy (S^{o}_{m}) and enthalpy changes (ΔH^{o}_{m}) for CbzLPG molecule were computed from the theoretical harmonic frequencies (Table-5). Table-5 depicts that the entropies, heat capacities and enthalpy changes were increasing with temperature ranging from 100 to 1000 K due to the fact that the molecular vibrational intensities increase with temperature [71]. These observed relations of the thermodynamic functions *vs.* temperatures were fitted by quadratic formulae and the corresponding fitting regression factors (R^2) is 0.963, 0.994 and 0.974 for heat capacity, entropy and enthalpy changes, respectively. The correlation graphics of temperature dependence on thermodynamic functions of CbzLPG molecule are shown in Fig. 9. Vibrational zero-point energy of the molecule CbzLPG is 721.93 kJ/mol.

Molecular docking: The molecular docking study is an essential tool in the pharmaceutical drug discovery [72]. The three-dimensional (3D) structural coordinates of the N-carbo-

TABLE-5
THERMODYNAMIC PROPERTIES AT DIFFERENT TEMPERATURES AT THE B3LYP/6-311 + G(d,p) LEVEL FOR N-CARBOBENZOXY-L-2-PHENYLGLYCINE

T (K)	S^0m (J mol^{-1} K^{-1})	$C^0_{p,m}$ (J mol^{-1} K^{-1})	ΔH^0m (KJ mol^{-1})
100.00	425.92	137.51	9.66
200.00	544.66	217.5	27.25
298.15	648.63	310.45	53.11
300.00	650.56	312.22	53.69
400.00	753.06	402.72	89.54
500.00	851.34	478.24	133.72
600.00	944.08	538.52	184.67
700.00	1030.84	586.66	241.02
800.00	1111.81	625.72	301.7
900.00	1187.43	657.94	365.94
1000.00	1258.19	684.87	433.12

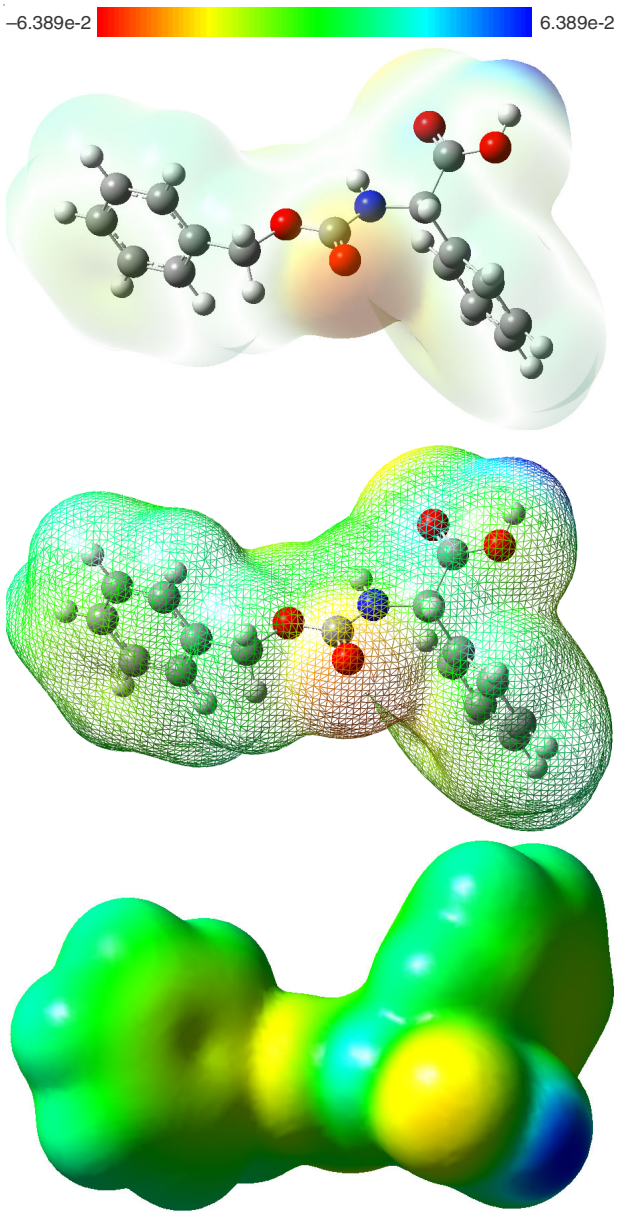

Fig. 8. Molecular electrostatic potential map (MEP) of N-carbobenzoxy-L-2-phenylglycine

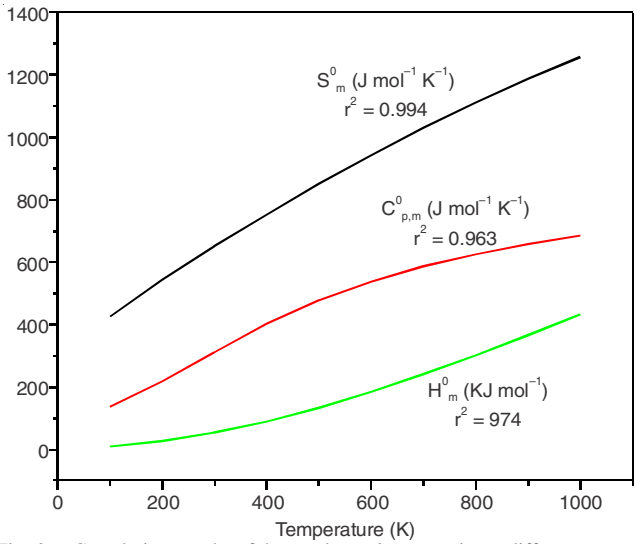

Fig. 9. Correlation graphs of thermodynamic properties at different temperature for N-Carbobenzoxy-L-2-phenylglycine

benzoxy-L-2-phenylglycine molecule were obtained from ChemSpider chemicals database [73]. The obtained structure was energy minimized using PRODRG online server on basis of GROMACS force field method [74-76]. In order to finding their potential target protein, we have used the PharmMapper server [77,78]. From the results, we have choose the SH2 domain of ^{pp60}Src with high affinity binding of full length inhibitors (PDB ID: 1O4R) for this docking study [79]. The 3D coordinates of protein file was downloaded from the RCSB protein data bank [80,81], the structure of target protein was determined by X-ray crystallography to 1.5 Å resolution. The protein preparation has been carried by following steps (i) all water molecules were removed (ii) hydrogen atoms were added to the crystal structure (ii) add Kollaman's charges (iii) previous docked inhibitor was removed from the protein. The AutoGrid 4.2 [82] was used to create affinity grids centered on the active site with 90 × 90 × 122 grid size with a spacing of 0.43 Å. The rigid protein and flexible ligand docking was performed by using AutoDock 4.2 with the Lamarckian genetic algorithm applying the following protocol: trials of 100 dockings, energy evaluations of 25000,000, population size of 200, a mutation rate of 0.02, a crossover rate of 0.8 and an elitism value of 1. The docking results were evaluated by sorting the binding free energy predicted by their docking confirmations, the best confirmation binding energy is predicted to be -8.52 kcal/mol and an elucidate the inhibition constant Ki to found to be 570.13 nM. This compound is formed hydrophobic interactions with ARG14, GLU37, THR38 and SER36 amino acid residues of ^{pp60}Src target protein. The specific interactions between ligand and target protein is shown in Fig. 10. The molecular docking result evidences for the biological activity of the ligand.

Conclusion

The molecular structural parameters of the optimized geometry of the compound N-carbobenzoxy-L-2-phenylglycine have been obtained from DFT (B3LYP and M06-2X) level of calculations. The computed geometries are benchmarks for predicting structural data of the molecule. The vibrational FT-IR and FT-Raman spectra of the CbzLPG were recorded and computed vibrational wavenumbers and their PED were calculated. A comparison between calculated vibrational spectra and their experimental counterpart showed a good correlation. Any variations located between the experimental and computed values is also considering that the computations had been carried out for a single molecule within the gas phase, whereas the experimental values within the solid phase had been recorded within the presence of intermolecular interactions. The performances of the B3LYP method of the prediction of the wavenumbers within the molecule were quite to closer than M06-2X level of calculations. The stable form of the title molecule was analyzed by the conformational stability analysis. A UV-visible spectral analysis of CbzLPG has been done by theoretical calculations. In order to understand electronic transitions to compound, TD-DFT calculations on electronic absorption spectra in gas phase and ethanol solvent were performed. The calculated HOMO and LUMO along with their plot has been presented for understanding of charge transfer occurring within the molecule. The NLO properties such as polarizabilities, the first hyperpolarizabilities and total dipole moment of the title compound have been calculated. The NLO properties revealed by theoretical calculations indicate that the compound may be good candidates of nonlinear optical materials, since they have quite large first hyperpolarizability values when compared to urea. The NBO analysis performed in this study enabled us to know about the conjugative interactions and other type of interactions taking place within the molecular species. Based on the frequencies scaled and the principle of statistic thermodynamics, thermodynamic properties ranging from 100 to 1000 K were obtained and it is obvious that, the gradients of C^0_p and S^0_m to the temperature decrease, but that of ΔH^0_m increases, as the temperature increases. The results prove the ability of the methodology (DFT) for elucidation of vibrational spectra of the title molecule and exceptional understanding of thermodynamic properties, NLO and NBO properties are helpful for the design and synthesis of new materials. The present quantum chemical study may examines further play and crucial role about knowledge of the structure, activity and dynamics of the molecule. The docking results

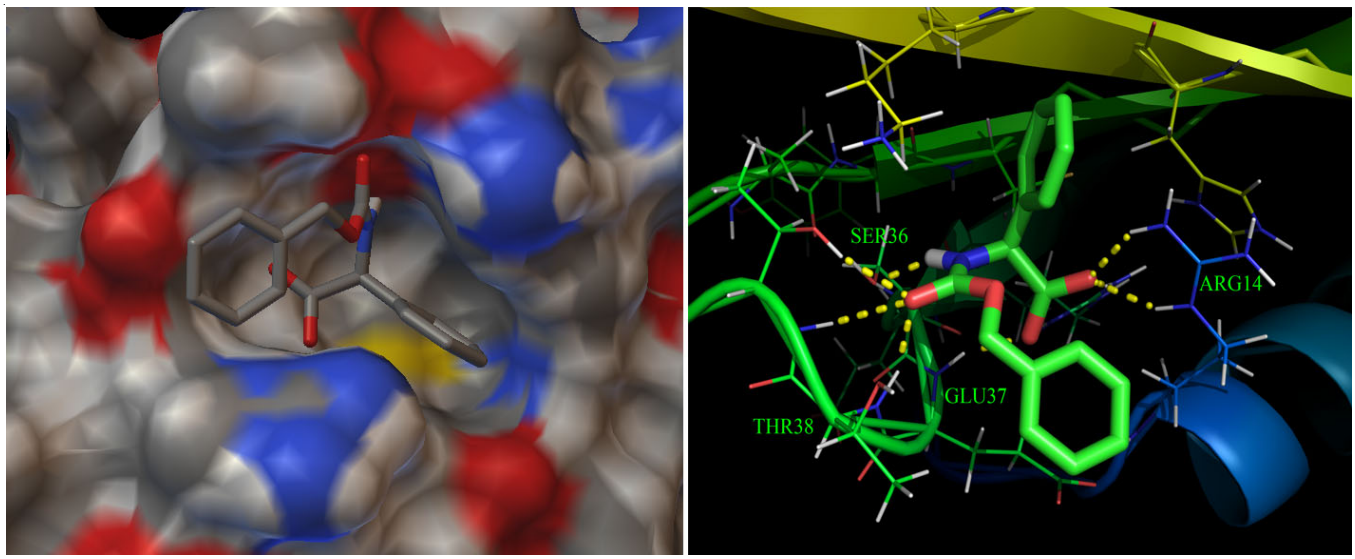

Fig. 10. Specific interactions of ligand with target amino acid residues of ^{pp60}Src

were evaluated by sorting the binding free energy predicted by their docking confirmations, the best confirmation binding energy is predicted to be -8.52 kcal/mol and an elucidate the inhibition constant K_i to found to be 570.13 nM. This compound is formed hydrophobic interactions with ARG14, GLU37, THR38 and SER36 amino acid residues of ^{pp60}Src target protein.

REFERENCES

1. J.L. Lynch III, P. Honore, D.J. Anderson, W.H. Bunnelle, K.H. Mortell, Ch. Zhong, C.L. Wade, Ch.Z. Zhu, H. Xu, K.C. Marsh, Ch.-H. Lee, M.F. Jarvis and M. Gopalakrishnan, *Pain*, **125**, 136 (2006).
2. A. Boto, J.A. Gallardo, R. Hernandez, F. Ledo, A. Munoz, J.R. Murguia, M. Menacho Marquez, A. Orjales and C.J. Saavedra, *Bioorg. Med. Chem. Lett.*, **16**, 6073 (2006).
3. O. Angelova, R. Petrova, V. Radomirska and T. Kolev, *Acta Crystallogr.*, **52C**, 2218 (1996).
4. S. Ravichandran, J.K. Dattagupta and Ch. Chakrabarti, *Acta Crystallogr.*, **54C**, 499 (1998).
5. N. Srinivasan, B. Sridhar and R.K. Rajaram, *Acta Crystallogr.*, **57E**, 754 (2001).
6. S. Ramaswamy, B. Sridhar, V. Ramakrishnan and R.K. Rajaram, *Acta Crystallogr.*, **57E**, 1149 (2001).
7. K. Bouchouit, L. Bendheif and N. Benali-Cherif, *Acta Crystallogr.*, **60E**, 272 (2004).
8. S. Bouacida, H. Merazig and P. Benard-Rocherulle, *Acta Crystallogr.*, **62E**, o838 (2006).
9. Y.J. Mast, W. Wohlleben and E. Schinko, *J. Biotechnol*., **155**, 63 (2011).
10. M. Kusano, K. Yasukawa and K. Inouye, *Enzyme Microb. Technol.*, **46**, 320 (2010).
11. M.M. Ilczyszyn, T. Lis and M. Wierzejewska, *J. Mol. Struct.*, **937**, 2 (2009).
12. M.M. Ilczyszyn, T. Lis, M. Wierzejewska and M. Zatajska, *J. Mol. Struct.*, **919**, 303 (2009).
13. M.A. Palafox, V.K. Rastogi, R.P. Tanwar and L. Mittal, *Spectrochim. Acta A*, **59**, 2473 (2003).
14. S. Mohan, N. Sundaraganesan and J. Mink, *Spectrochim. Acta A*, **47**, 1111 (1991).
15. G.N. Ten, V.V. Nechaev, A.N. Pankratov, V.I. Berezin and V.I. Baranov, *J. Struct. Chem.*, **51**, 854 (2010).
16. C. Cirak and N. Koc, *J. Mol. Model.*, **18**, 4453 (2012).
17. M.A. Palafox, G. Tardajos, A. Guerrero-Martínez, V.K. Rastogi, D. Mishra, S.P. Ojha and W. Kiefer, *Chem. Phys.*, **340**, 17 (2007).
18. M. Szczesniak, M.J. Nowak, K. Szczepaniak and W.B. Person, *Spectrochim. Acta A*, **41**, 237 (1985).
19. J.S. Singh, *J. Mol. Struct.*, **876**, 127 (2008).
20. M.H. Jamróz, J.C. Dobrowolski and R. Brzozowski, *J. Mol. Struct.*, **787**, 172 (2006).
21. C. Cirak, Y. Sert and F. Ucun, *Spectrochim. Acta A*, **92**, 406 (2012).
22. Y. Zhao and D.G. Truhlar, *Theor. Chem. Acc.*, **120**, 215 (2008).
23. K. Helios, R. Wysokinski, A. Pietraszko and D. Michalska, *Vib. Spectrosc.*, **55**, 207 (2011).
24. J. Gu, J. Wang and J. Leszczynski, *Chem. Phys. Lett.*, **512**, 108 (2011).
25. K.H. Lemke and T.M. Seward, *Chem. Phys. Lett.*, **573**, 19 (2013).
26. E.I. Paulraj and S. Muthu, *Spectrochim. Acta A*, **108**, 38 (2013).
27. U. Yadava, M. Singh and M. Roychoudhury, *Comput. Theor. Chem.*, **977**, 134 (2011).
28. C.N. Ramachandran and E. Ruckenstein, *Comput. Theor. Chem.*, **973**, 28 (2011).
29. Y. Sert, C. Cirak and F. Ucun, *Spectrochim. Acta A*, **107**, 248 (2013).
30. M.J. Frisch, *et al*., Gaussian 09, Revision A.1, Gaussian, Inc., Wallingford CT (2009).
31. P. Hohenberg and W. Kohn, *Phys. Rev.*, **136**, B86 (1964).
32. A.D. Becke, *J. Chem. Phys.*, **98**, 5648 (1993).
33. C. Lee, W. Yang and R.G. Parr, *Phys. Rev. B*, **37**, 785 (1988).
34. E. Frisch, H.P. Hratchian, R.D. Dennington II, T.A. Keith, J. Millam, B. Nielsen, A.J. Holder and J. Hiscocks. Gaussian, Inc. GaussView Version 5.0.8 (2009).
35. M.H. Jamroz, Vibrational Energy Distribution Analysis: VEDA 4 Program, Warsaw, Poland (2004).
36. Y. Morino and K. Kuchitsu, *J. Chem. Phys.*, **20**, 1809 (1952).
37. W.J. Taylor, *J. Chem. Phys.*, **22**, 1780 (1954).
38. T. Miyazawa, T. Shimanouchi and S. Mizushima, *J. Chem. Phys.*, **29**, 611 (1958).
39. G. Zerbi, J. Overend and B. Crawford, *J. Chem. Phys.*, **38**, 122 (1963).
40. G. Keresztury and G. Jalsovszky, *J. Mol. Struct.*, **10**, 304 (1971).
41. P. Pulay, G. Fogarasi, F. Pang and J.E. Boggs, *J. Am. Chem. Soc.*, **101**, 2550 (1979).
42. L. Lapinski and P. Pongor, PED-Program, Warsaw, Poland (1994).
43. E.D. Glendening, C.R. Landis, F. Weinhold, *WIREs Comput. Mol. Sci*., **2**, 1 (2011).
44. D.A. Kleinman, *Phys. Rev.*, **126**, 1977 (1962).
45. S. Shen, G.A. Guirgis and J.R. Durig, *Struct. Chem.*, **12**, 33 (2001).
46. D. Michalska and R. Wysoki'nski, *Chem. Phys. Lett.*, **403**, 211 (2005).
47. D. Michalska, RAINT, A Computer Program for Calculation of Raman Intensities from the Gaussian Outputs, Wroclaw University of Technology, Poland (2002).
48. K. Dong and Y. Wang, *Acta Crystallogr.*, **70E**, o527 (2014).
49. V. Arjunan, T. Rani, C.V. Mythili and S. Mohan, *Spectrochim. Acta A*, **79**, 486 (2011).
50. D. Sajan, H.J. Ravindra, N. Misra and I.H. Joe, *Vib. Spectrosc.*, **54**, 72 (2010).
51. N.P.G. Roges, A Guide to the Complete Interpretation of the Infrared Spectra of Organic Structures, Wiley, New York (1994).
52. A. Fu, D. Du and Z. Zhou, *Spectrochim. Acta*, **59**, 245 (2003).
53. K. Govindarasu and E. Kavitha, *Spectrochim. Acta*, **133**, 799 (2014).
54. L.D. Stefano, R. Cioffi and F. Colangelo, *J. Anal. Chem.*, **3**, 1 (2012).
55. L.J. Bellamy, The Infrared Spectra of Complex Molecules, Chapman and Hall, London (1980).
56. N.B. Colthup, L.H. Daly and S.E. Wiberley, Introduction to Infrared and Raman Spectroscopy, Academic Press, New York (1990).
57. R.M. Silverstein, G.C. Bassler and T.C. Morril, Spectrometric Identification of Organic Compounds, John Wiley & Sons Inc., Singapore, edn 5 (1991).
58. A. Spire, M. Barthes, H. Kellouai and G. De Nunzio, *Physica D*, **137**, 392 (2000).
59. C.Y. Panicker, H.T. Varghese and T. Tansani, *Turk. J. Chem.*, **33**, 1 (2009).
60. A.E. Reed, L.A. Curtiss and F. Weinhold, *Chem. Rev.*, **88**, 899 (1988).
61. J. Henriksson, T. Saue and P. Norman, *J. Chem. Phys.*, **128**, 024105 (2008).
62. J.P. Hermann, D. Ricard and J. Ducuing, *Appl. Phys. Lett.*, **23**, 178 (1973).
63. S. Debrus, H. Ratajczak, J. Venturini, N. Pincon, J. Baran, J. Barycki, T. Glowiak and A. Pietraszko, *Synth. Met.*, **127**, 99 (2002).
64. K. Govindarasu and E. Kavitha, *Spectrochim. Acta A*, **122**, 130 (2014).
65. R. Parr, L. Szentpaly and S. Liu, *J. Am. Chem. Soc.*, **121**, 1922 (1999).
66. P.K. Chattaraj, B. Maiti and U. Sarkar, *J. Phys. Chem. A*, **107**, 4973 (2003).
67. R. Parr, R. Donnelly, M. Levy and W. Palke, *J. Chem. Phys.*, **68**, 3801 (1978).
68. R. Parr and R. Pearson, *J. Am. Chem. Soc.*, **105**, 7512 (1983).
69. R.G. Parr and P.K. Chattaraj, *J. Am. Chem. Soc.*, **113**, 1854 (1991).
70. T.A. Koopmans, *Physica*, **1**, 104 (1934).
71. Z. Ran, D. Baotong, S. Gang and S. Yuxi, *Spectrochim. Acta*, **75A**, 1115 (2010).
72. W.L. Jorgensen, *Science*, **303**, 1813 (2004).
73. Chemspider chemical structure database http://www.chemspider.com/Chemical-Structure.715749.html (accessed on 12 December 2015).
74. D.M.F. van Aalten, R. Bywater, J.B.C. Findlay, M. Hendlich, R.W.W. Hooft and G. Vriend, *J. Comput. Aided Mol. Des.*, **10**, 255 (1996).
75. A.W. Schüttelkopf and D.M.F. van Aalten, *Acta Crystallogr. D Biol. Crystallogr.*, **60**, 1355 (2004).
76. The GlycoBioChem PRODRG2 Server http://davapc1.bioch.dundee.ac.uk/cgi-bin/prodrg/ (accessed on 08 January 2016).
77. X. Liu, S. Ouyang, B. Yu, Y. Liu, K. Huang, J. Gong, S. Zheng, Z. Li, H. Li and H. Jiang, *Nucleic Acids Res.*, **38(Web Server)**, W609 (2010).
78. PharmMapper Server http://59.78.96.61/pharmmapper/ (accessed on 08 January 2016).
79. G. Lange, D. Lesuisse, P. Deprez, B. Schoot, P. Loenze, D. Bénard, J.P. Marquette, P. Broto, E. Sarubbi and E. Mandine, *J. Med. Chem.*, **46**, 5184 (2003).
80. H.M. Berman, J. Westbrook, Z. Feng, G. Gilliland, T.N. Bhat, H. Weissig, I.N. Shindyalov and P.E. Bourne, *Nucleic Acids Res.*, **28**, 235 (2000).
81. RCSB The Protein Data Bank http://www.rcsb.org/ (accessed on 08 January 2016).
82. G.M. Morris, D.S. Goodsell, R.S. Halliday, R. Huey, W.E. Hart, R.K. Belew and A.J. Olson, *J. Comput. Chem.*, **19**, 1639 (1998).